STUK

STUK-YTO-TR 175 February 2001

SPENT BWR FUEL CHARACTERISATION COMBINING A FORK DETECTOR WITH GAMMA SPECTROMETRY

Raport on Task JNT A 1071 FIN of the Finnish Support Programme to IAEA Safeguards

A. Tiitta, J. Hautamäki
VTT Chemical Technology
A. Turunen
STUK
R. Arlt, J. Arenas Carrasco, K. Esmailpour-Kazerouni
IAEA
P. Schwalbach
Euratom Safeguards Office

STUK • SÄTEILYTURVAKESKUS • STRÅLSÄKERHETSCENTRALEN
RADIATION AND NUCLEAR SAFETY AUTHORITY

The conclusions presented in the STUK report series are those of the authors and do not necessarily represent the official position of STUK.

ISBN 951-712-436-8
ISSN 0785-9325

Oy Edita Ab, Helsinki 2001

TIITTA Antero, HAUTAMÄKI Johanna (VTT Chemical Technology), TURUNEN Asko, (STUK), ARLT Rolf, ARENAS CARRASCO Jose, ESMAILPOUR-KAZEROUNI K (IAEA), SCHWALBACH Peter (Euratom Safeguards Office). Spent BWR fuel characterisation combining a fork detector with gamma spectrometry. Raport on Task JNT A 1071 FIN of the Finnish Support Programme to IAEA Safeguards. STUK-YTO-TR 175. Helsinki 2001. 37 pp. + Annexes 8 pp.

ISBN 951-712-436-8
ISSN 0785-9325

Keywords: spent fuel, partial defect, fork detector, NDA, safeguards

ABSTRACT

The LWR spent fuel assemblies have to be verified at the partial defect level before they become difficult to access. According to the IAEA's criteria the partial defect test for spent fuel should be able to detect if half or more of the fuel pins have been removed from an assembly and possibly replaced by dummies. Euratom applies similar criteria. Therefore a standard verification procedure needs to be developed using an appropriate combination of measurements and theoretical calculations.

Two experiments with an "upgraded" fork detector were performed at the TVO KPA Store in September and in December 1999. On the whole, 26 assemblies were measured.

In the "upgraded" fork detector the total neutron count and the gross gamma measurements are complemented with gamma spectroscopic measurement using an integrated measurement head. A cadmium–zinc–telluride (CZT) detector is placed on the same vertical level as the fission and ionisation chambers. This enables simultaneous gamma and neutron measurements at one location. In the upgraded fork model the fork prongs can also be removed and gamma spectrometric measurements can be done using only the CZT detector. This allows more versatile placement of the target fuel assembly allowing various kind of gamma spectroscopic scanning measurements.

In this report a gamma spectroscopy based correction to the gross gamma data is introduced. This corrected gross gamma signal seems to describe more consistently the burnup of the assembly than the ^{137}Cs intensity obtained by direct gamma spectrometry.

Concerning the measured neutron data of assemblies with different enrichments, an enrichment correction method based on calculations made with the ORIGEN-S program is introduced in this report. In addition, the share of ^{244}Cm neutrons of the total neutron source is derived from the results calculated with the PYVO program. These corrections to the neutron signal seem to improve the correlation of the neutron signal to the burnup and to the gross gamma signal.

The PYVO program can be considered as an essential tool in the analysis. With help of the PYVO the ^{244}Cm share of total neutron counts, the ^{244}Cm neutron source term and the ^{137}Cs activity of measured assemblies can be calculated.

In addition, the axial activity profiles of one assembly are compared with the calculations made by ORIGEN-S. These comparisons show a remarkable agreement between the measured and calculated results.

CONTENTS

1 INTRODUCTION

The requirement for partial defect test applies to irradiated fuel assemblies, which can be dismantled at the facility. According to the IAEA's criteria the partial defect test for spent fuel should be able to detect if half or more of the fuel pins have been removed from an assembly and possibly replaced by dummies. The verification method investigated in this report is passive neutron counting combined with gamma spectroscopy. The verification should show consistency between the operator-declared fuel-assembly characteristics and the measured neutron and gamma ray data.

The partial defect test method for LWR spent fuel assemblies as presently recommended in the safeguards criteria requires a combination of passive neutron assay (PNA) using the fork Detector (FDET) and high resolution gamma spectrometry with HPGe detectors (GBUV). However, the use of liquid nitrogen cooled germanium detectors in spent fuel ponds, is impractical and the method is not used as recommended.

The use fork detector and its capability to reveal missing pins in the case of a deliberate falsification of the operator's data have earlier extensively studied by Rinard and Bosler [1]. The technological development during the last decade has introduced new tools, and one should consider how these new developments could be used to complement and improve the data obtainable by a fork detector.

The quality of cadmium–zinc–telluride (CZT) detectors has been developed in Latvia and in the US. Recently, the resolution of CZT detectors has been improved to such an extent, that they can replace the more difficult to use HPGe detectors in certain spent fuel gamma measurements. This could allow, for the first time, the design of a compact underwater partial defect verification device for LWR spent fuel assemblies. The device is built around the fork detector concept.

In November 1998, a first test of a prototype system was conducted under the IAEA Task JNT 1077 in the KPA Store in Olkiluoto (Finland). The quality of the gamma spectra was excellent, allowing—using specialised software developed under the US MSSP—to extract the needed information, with a quality characteristic to a liquid–nitrogen cooled HPGe detector. However, the observed scatter of the data points of the neutrons vs. measured activity of ^{137}Cs correlation curve was high in the November 98 measurements and suggestions were made to improve the design of the device to allow a better control of the measurement geometry. Based on this, the Finnish MSSP took up a task to redesign the fork detector, integrating it completely with a compact CdZnTe based underwater gamma spectrometer to reduce error sources due to assembly positioning. Two measurement campaigns were performed under Task JNT A 1071 FIN "Partial Defect Test on Spent Fuel LWRs" in the KPA Store in Olkiluoto in September and in December 1999.

The measurement system is introduced in section 2 and the measurements are described in section 3. The angular gamma spectroscopic scanning and the sensitivity to horizontal positioning are analysed in sections 4 and 5. The measurements performed on one vertical level of the assembly are analysed in section 6. The axial scanning measurements are presented in section 7. The sensitivity to vertical positioning and the influence of the vertical irradiation profile variation are considered in section 8. Finally, some conclusions based on the analysis of the measurement results are drawn in section 9.

2 MEASUREMENT SYSTEM

2.1 Electrical components

The equipment used in the measurements is based on a standard IAEA BWR fork detector concept with a special upgrade, which integrates into the device a CZT detector and a collimator assembly for gamma spectroscopic measurements. The main parts of the detector head, without the cabling, are presented in Figure 1.

The fork detector part of the instrument consists of four fission chambers, type Reuter–Stokes RS-P6-0805-134, for neutron detection and two ionisation chambers, type LND 52113, for gross gamma measurement. The detectors are positioned symmetrically inside two detachable polyethylene prongs, which are on opposite sides of the assembly to be measured.

Two of the fission chambers are inside cadmium wrapping and the remaining two fission chambers are outside the cadmium wrapping. The similar neutron detectors, i.e. the cadmium wrapped fission chambers and the bare fission chambers are connected pairwise together. The two cables carrying the neutron signals are connected to a lead shielded amplifier-discriminator module PDT210A of Precision Data Technology. PDT210A is designed for high radiation environment. It contains two signal channels consisting of a charge-sensitive preamplifier, a shaping amplifier and a discriminator, and it produces a logical pulse for each detected neutron. A GRAND 3 is used for biasing the fission chambers and for powering the amplifier–discriminator unit. It is also used for counting and displaying the neutron counts from the fission chambers.

The ionisation chambers are also connected together to produce the sum of the ion currents of each chamber. The GRAND 3 is used for biasing the ionisation chambers and for measuring and displaying the ion current.

A CZT detector, type SDP 310/Z/20S (Ritec Ltd., Riga, Latvia), is used to measure the gamma-ray spectrum emitted by the fuel assembly. This detection device consists of a probe and a cable with connector. The probe contains a single 20 mm^3 CZT detector and a charge-sensitive preamplifier. The preamplifier output impedance is 50 ohms and it can drive a 50 ohm cable up to 20 metres. An important characteristic of this device is its room temperature operation. The gamma

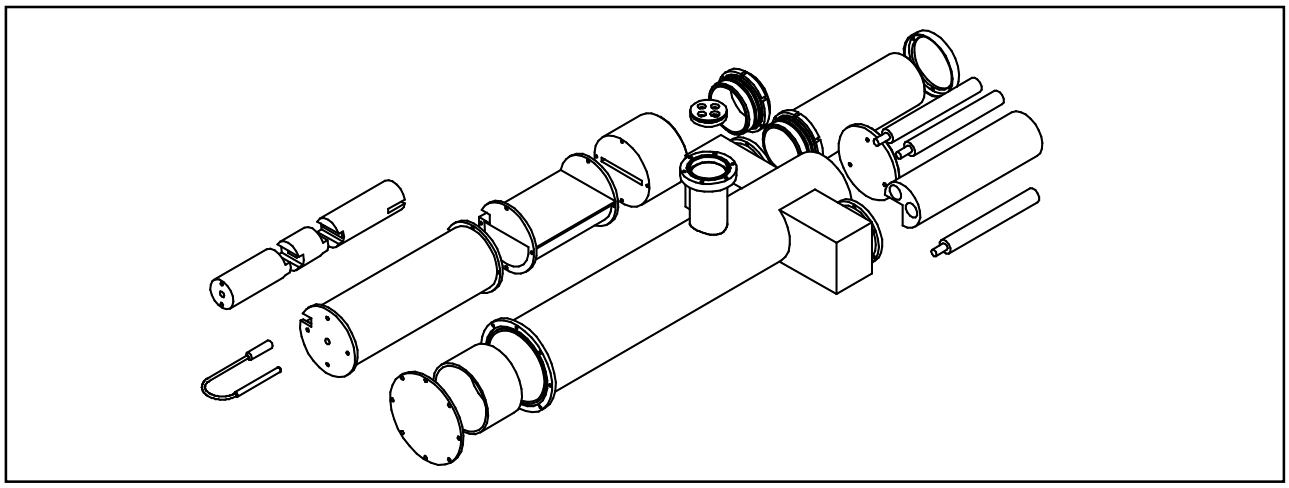

Figure 1. *Main components of the detector head.*

ray spectrum from the CZT detector is recorded by an Ortec DART multi-channel analyser (MCA). A portable PC with the SAMPO 90 measurement control and spectrum analysing program is used to get the essential data of measured spectra. A block scheme of the measurement system is presented in Figure 2.

2.2 Mechanical construction

The detector head contains the fork detector with detachable prongs and the collimator housing including the lead-shielded CZT detector with a steel collimator (see Figure 1). A cross-section of the detector head is presented in Figure 3. The main

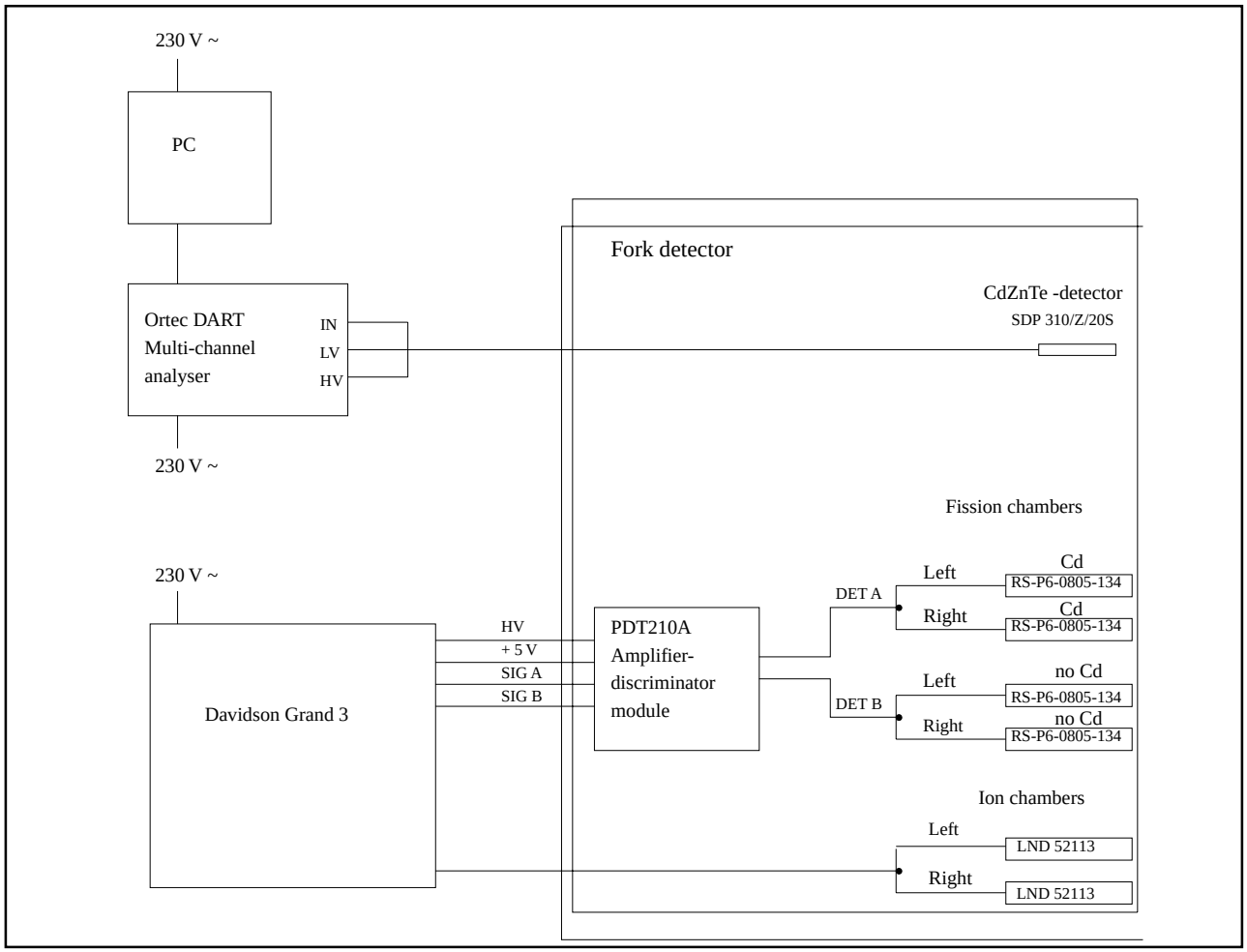

Figure 2. *Block scheme of the measurement system.*

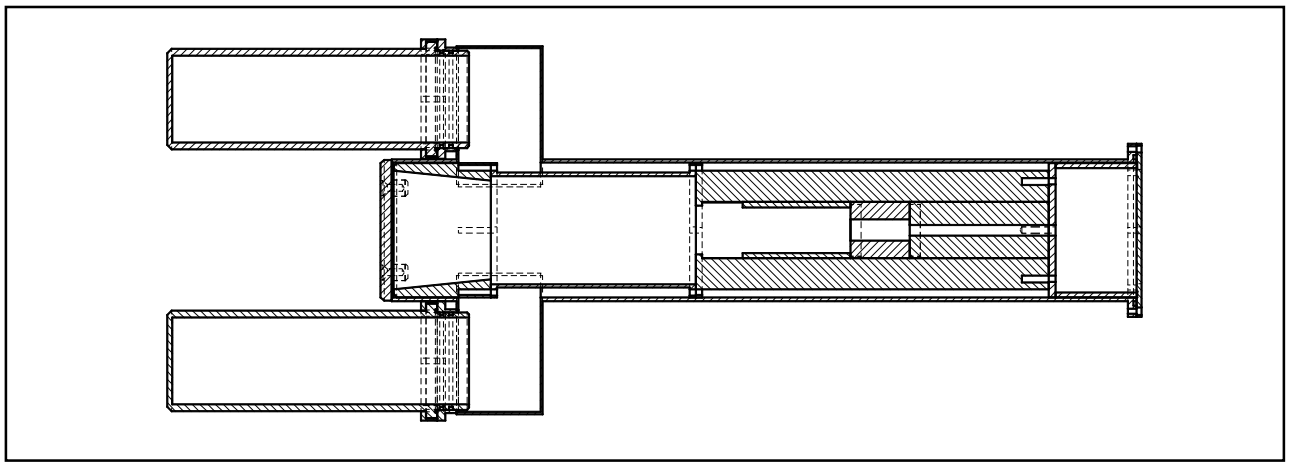

Figure 3. *A cross-section of the detector head. The fission chambers, the ion chambers and the CZT detector are not presented in this drawing.*

mechanical components of the detector head are also presented in Figure 5. The opening between the prongs is nominally 149 mm whereas the thickness of the assembly with a fuel channel is nominally 139 mm.

The rear end of the collimator housing is enclosed by a blind flange. The detector head forms a closed watertight package, which is connected by a flange joint to a 350 mm long vertical amplifier housing, which contains the PDT210A module in a lead shield. All joints are sealed with o-rings to make the joints watertight. All flanges are fixed with acid resisting stainless steel screws. The polyethylene prongs are fixed with screws using a fixing steel ring to provide an even compression to the flange of the polyethylene prong.

An 8 m long vertical pipe consisting of four 2 m long sections holds the detector head during the measurements and brings the dry cables from the pond up to the floor level. The pipe sections are connected to each other by screw joints sealed with o-rings. An extra 1 m long section is provided to adjust the height of the vertical pipe at 1 metre intervals (7, 8 or 9 metres).

The vertical pipe is fixed in the periscope console in the edge of the pond (Figure 4 and Figure 5). In order to keep the measurement system in a fixed position, there is a direction rail in the periscope console and a collar is attached to the uppermost pipe section. The collar is wide enough that the measurement system cannot drop into the pond. The guide plate of the collar prevents the measurement system from rotating in the guide rail. In addition to this, a safety chain connected to the pond railing holds the pipe in order to ensure that the measurement system cannot be dropped into the pond should the pipe become unfastened from the periscope console. The height and angle of the fixing in the console is adjustable. The accurate fixing point can be defined with the help of the scale of the uppermost pipe section.

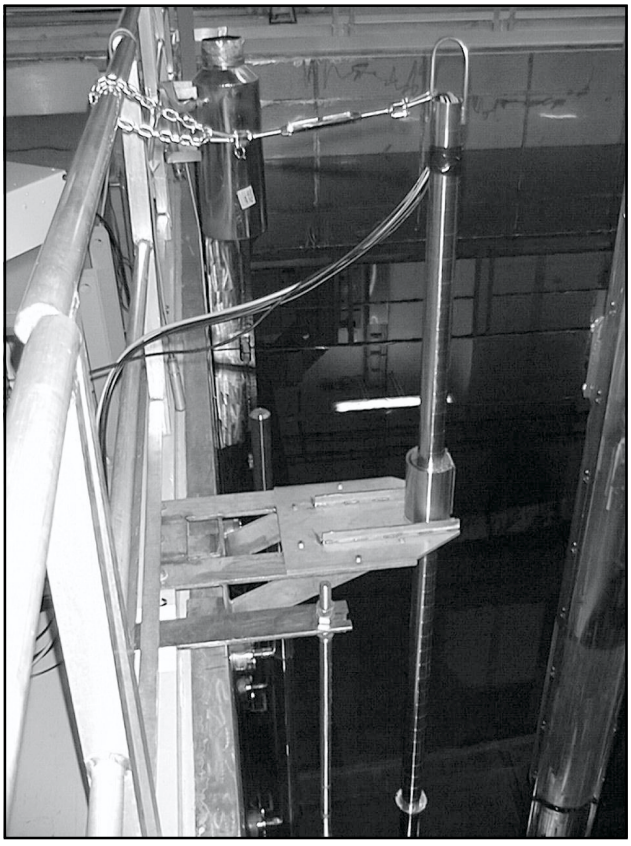

Figure 4. *Fastening of the vertical pipe in the periscope console.*

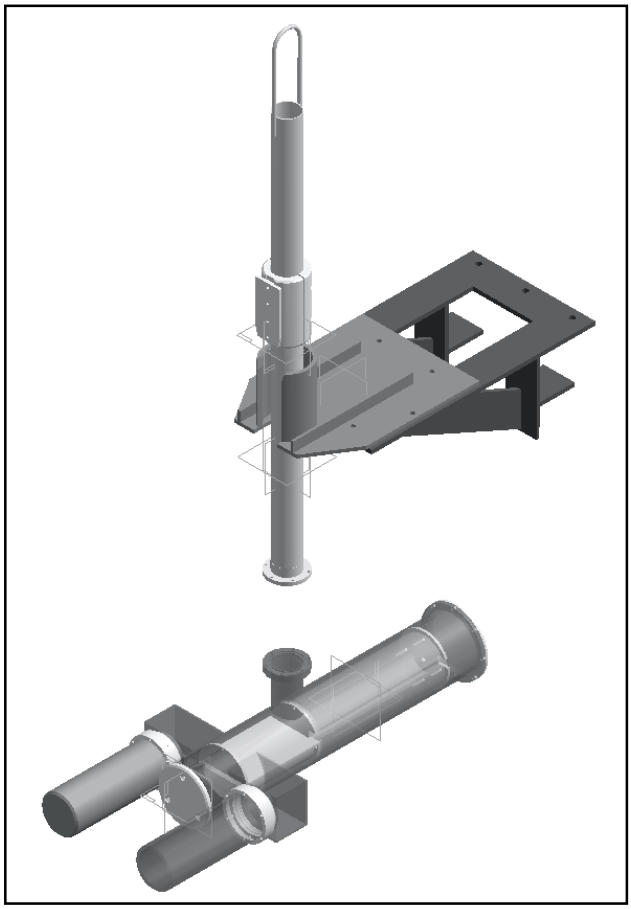

Figure 5. *Fastening of the vertical pipe in the periscope console and the main mechanical components of the detector head. The safety chain is not presented in this picture.*

2.3 Comparison between the first fork detector and the upgraded fork detector

There are a few important differences between the first fork test detector with a “trumpet” and the upgraded one. In the first version the CZT detector was about 400 mm above the fission and ionisation chambers. In other words, two measurements are needed to get data points of one axial position of the assembly. [2] In the “upgraded” fork detector the CZT detector is on the same vertical level as the fission and ionisation chambers. Because of this, gamma and neutron measurements can be done simultaneously at one vertical level of the fuel assembly. In the upgraded fork model the fork prongs can also be removed and gamma-spectrometric measurements can be performed using only the CZT detector. The first system design used in the November 1998 measurements is presented in Figure 6 and the upgraded one in Figures 7 and 8.

2.4 Software

The gamma ray spectrum from the CZT detector, recorded by DART, was analysed with the help of the analysing program SAMPO [3]. In addition, an analysing program CsRatio [4] was used to compare results of SAMPO in the measurements performed in September.

The measurement results were collected to Excel spreadsheets, which were prepared for this purpose beforehand. In addition to this, some preliminary data handling was done with the help of Excel on the spot to assess the quality of the data. The final analysis including theoretical activity calculations and curve fitting was done with help of the programs SigmaPlot [5], PYVO and ORIGEN-S [6]. PYVO is a lightened version of the CESAR code [7]. Measurement devices that include the PYVO code have been described in references 8, 9 and 10.

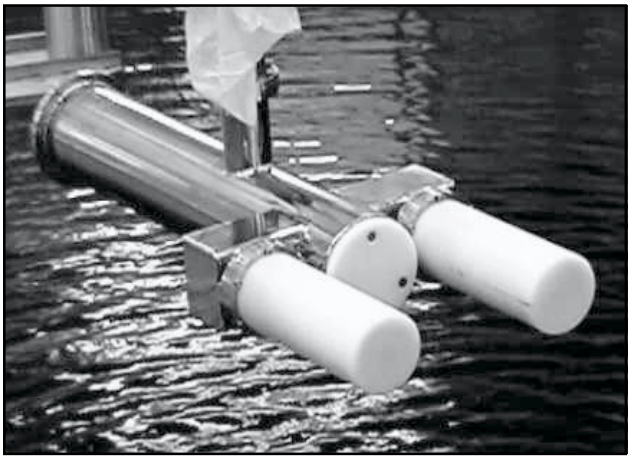

Figure 7. *Upgraded fork detector with prongs.*

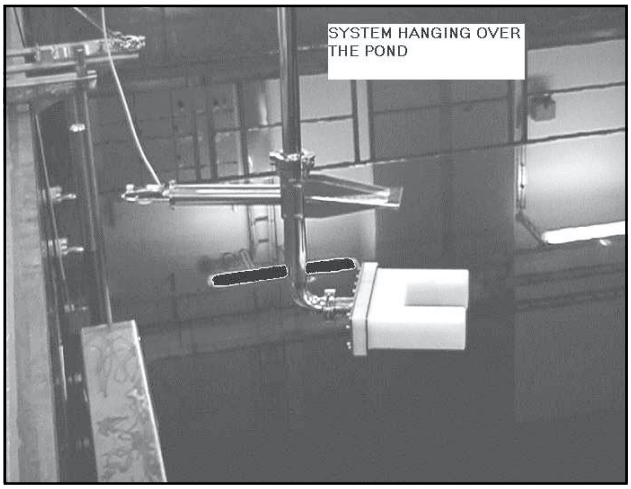

Figure 6. *The first modification to the fork detector used in the November 1998 measurements. [2]*

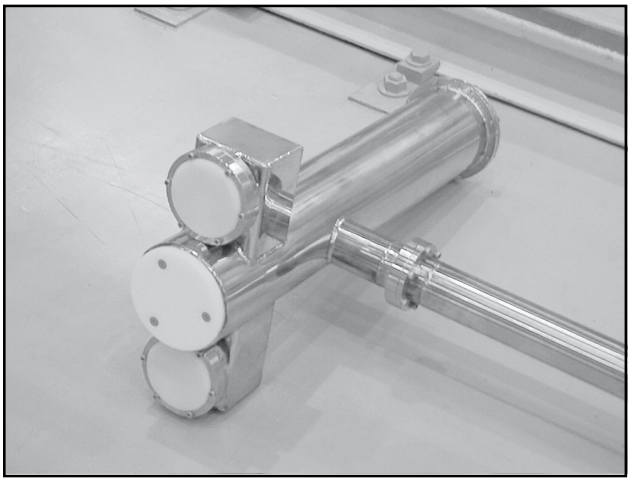

Figure 8. *Upgraded fork detector without prongs.*

3 MEASUREMENTS

3.1 Fuel data

The total number of measured assemblies was 26. Sixteen assemblies were measured during the first campaign (no. 1–16 in Table I) and eleven during the second campaign (no. 17–27 in Table I). The assembly #12323 was measured in both campaigns. All assemblies except for the assemblies #7289 and #13285 have been irradiated in 3–5 sequential one-year cycles. The assemblies #7289 and #13285, which were measured during the second campaign, have had an intermediate one-year off-reactor cycle.

3.2 The first measurement campaign

On every measurement day the functioning of the neutron measurement system was tested with help of an Am–Be neutron source, which was mounted in an assembly shaped box. The neutron source was lowered into the pond, and the signals of both the cadmium wrapped and the bare fission chambers were taken. These neutron count rates were found to be constant throughout the measurements.

The assemblies to be measured were brought from the storage pond to the evacuation pond by the fuel handling machine. The accurate positioning of the fuel assembly between the prongs of the fork was made with the fuel handling machine and the detector head was kept in a fixed position.

Angular gamma spectroscopic scanning of assembly #12350 was performed using only the CZT detector with the fork prongs removed. The assembly was rotated 95º clockwise and the scanning was taken at 5º intervals (i.e. 20 points). To check the sensitivity to repositioning of an assembly some measurements were repeated at some measurement positions. All other measurements were performed with the fork prongs attached, and the total neutron count, the gross gamma current and the gamma spectrum were taken.

The assembly #12350 was moved horizontally towards the measurement head and measured at 10 mm intervals in the central part of the assembly (z = 5705 mm). The first measurement point (x = 0 mm) corresponds to a situation, when the farthest side of the assembly was in line with the end of the fork prong (Figure 9). The nearest position to the measurement head corresponds to a situation, when x-coordinate was –40 mm (Distance from the collimator end plate was about 10 mm.)

In the axial scanning measurements and in the measurements taken at one vertical level the horizontal coordinate x = 0 mm was used.

The total neutron, the gross gamma and the gamma spectrum of assemblies no. 1–16 listed in Table I were measured in the central part of the assembly, at x = 0 mm and z = 5705 mm (Figure 9). The assemblies were measured at four sides with 90 degrees rotation to even up possible azimuthal asymmetry.

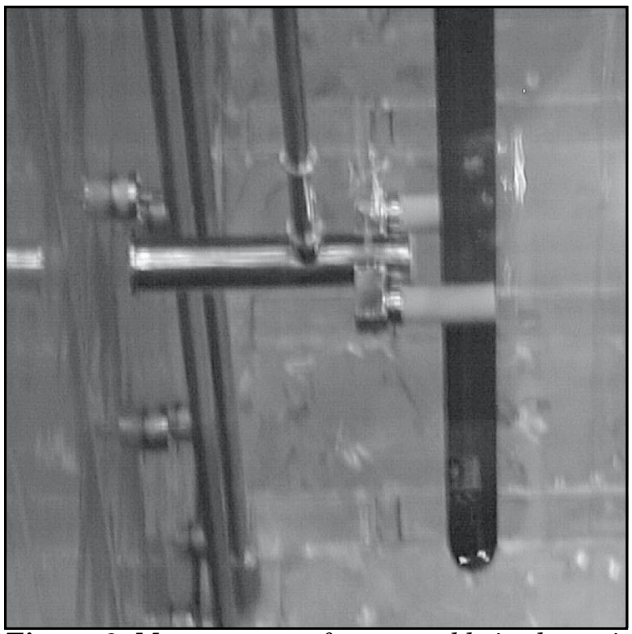

Figure 9. *Measurement of an assembly in the position (x,z) = (0 mm, 5705 mm). The farthest side of the assembly is in line with the end of the fork prong. There is a large water gap between the assembly and the collimator end plate.*

Table I. *List of the measured assemblies. The type code 8 denotes the ABB 8×8-1 assembly, the type code 9 the Siemens 9×9-1 assembly and S-64 the ABB SVEA-64 assembly.*

No.	Ass. ID	Type	IE (%)	Initial mass of U (kg)	No of reactor cycles	Off-reactor cycles	BU (MWd/kg)	Date of evacuation from reactor	CT (days) as of 1.9 or 8.12.1999	Location
1	7055	8	1.94	177.8	4		17.717	3.7.1983	5904	01B06
2	7516	8	2.81	177.3	3		26.228	10.6.1985	5196	41B28
3	7472	8	2.81	177.3	3		25.888	11.6.1985	5195	12B01
4	12500	8	2.94	177.5	3		28.524	3.5.1988	4138	50B01
5	12387	8	2.95	177.6	3		28.802	6.5.1988	4135	51B37
6	10181	8	2.94	177.5	4		34.590	8.5.1990	3403	09B01
7	12350	8	2.94	177.6	4		35.370	17.5.1991	3029	39B06
8	12366	8	2.95	177.7	4		31.966	4.5.1989	3772	03B06
9	10475	8	2.95	177.3	4		27.615	5.5.1988	4136	52B42
10	12323	8	2.95	177.5	4		33.965	30.5.1990	3381	44B14
11	6124	8	2.74	177.7	5		37.816	10.6.1985	5196	42B14
12	10003	8	2.90	178.2	4		27.815	5.5.1988	4136	47B25
13	9367	8	2.90	177.6	4		29.961	26.5.1988	4115	44B05
14	12338	8	2.97	177.5	4		32.953	30.5.1990	3381	44B42
15	13857	S-64	2.95	181.0	4		33.067	20.4.1991	3056	01B03
16	0104	9	3.00	172.8	3		30.948	23.5.1989	3753	36B40
17	4468	8	1.938	174.2	4		14.98	18.5.1982	6413	13A08
18	4469	8	1.938	178.0	4		16.64	21.5.1982	6410	13A23
19	7121	8	1.936	178.0	5		18.881	11.5.1984	5689	25A20
20	7289	8	1.939	177.5	5	83-84 (1)	20.981	8.5.1985	5327	23A22
21	7543	8	2.816	177.8	3		23.353	11.6.1985	5293	13A18
22	6110	8	2.747	177.7	3		25.03	22.5.1983	6044	18A32
23	10048	8	2.91	177.7	4		28.282	5.5.1988	4234	23B06
24	13285	8	3.027	178.0	5	89-90 (1)	30.882	11.5.1993	2402	27B31
25	12323	8	2.952	177.5	4		33.965	30.5.1990	3479	44B14
26	16732	S-64	2.98	183.8	5		35.21	11.5.1996	1306	24B39
27	425	9	3.22	172.0	4		39.039	31.5.1993	2382	28B24

The fuel assemblies #6124 and #7055 were scanned axially at nine vertical positions (Table II).

To relate the DART MCA and SAMPO software used in these measurements to the MMCA and CsRatio software used in the first fork measurements in November 1998, most of the assemblies were also measured with the MMCA. These results were used to determine the ratio of the ^{137}Cs peaks, which should be independent of the analysing system if the MCA systems are compatible.

Table II. *Coordinates of the axial scanning.*

x (mm)	z (mm)
0	4382
0	4825
0	5268
0	5711
0	6154
0	6597
0	7040
0	7483
0	7926

3.3 The second measurement campaign

All measurements were performed with the fork prongs attached. Like in the first campaign, the horizontal coordinate x = 0 mm was used in all measurements

The total neutron count, the gross gamma current and the gamma spectrum of assemblies no. 17–27 listed in Table I were measured at three different heights, at z = 5135, 5705 and 6275. Like in the September campaign, the assemblies were measured at four sides with 90 degrees rotation. The assembly #12323, which had been measured in September, was remeasured to scale the measurement data of this campaign with the September campaign.

The fuel assembly #12323 was scanned axially at eleven vertical positions (Table III).

Table III. *Coordinates of the axial scanning.*

x (mm)	z (mm)
0	4375
0	4755
0	5135
0	5515
0	5705
0	5895
0	6275
0	6655
0	7035
0	7415
0	7795

4 ANGULAR GAMMA SPECTROSCOPIC SCANNING

The ^{137}Cs-signal (A_{37}) vs. the viewing angle was investigated with the assembly #12350. It was expected that due to square lattice of the rods there could be a shadowing effect at zero angle (one side of the assembly perpendicular to the viewing direction) when all other rods are shadowed by the first plane of rods. When tilted a little, the rods behind the first plane would become visible, and it is expected that there could be a minimum at zero angle. The results of the angular scanning are illustrated in Figure 10. Contrarily to the expectation, it was observed an antisymmetric oscillation at zero angle with the FWHM about 15°. The reason for this antisymmetry is not understood, yet. On the other hand, the activity ratio of ^{134}Cs to ^{137}Cs (A_{34}/A_{37}) vs. rotation angle seems to be almost independent of the rotation angle (Figure 10).

The measured raw data are shown in Table A1.I in Annex 1.

The steep dependence of the gamma spectrometrically measured ^{137}Cs peak intensity on the rotation angle close to zero angle, which would be the natural measurement geometry, makes it questionable to use the ^{137}Cs peak intensity to describe the burnup.

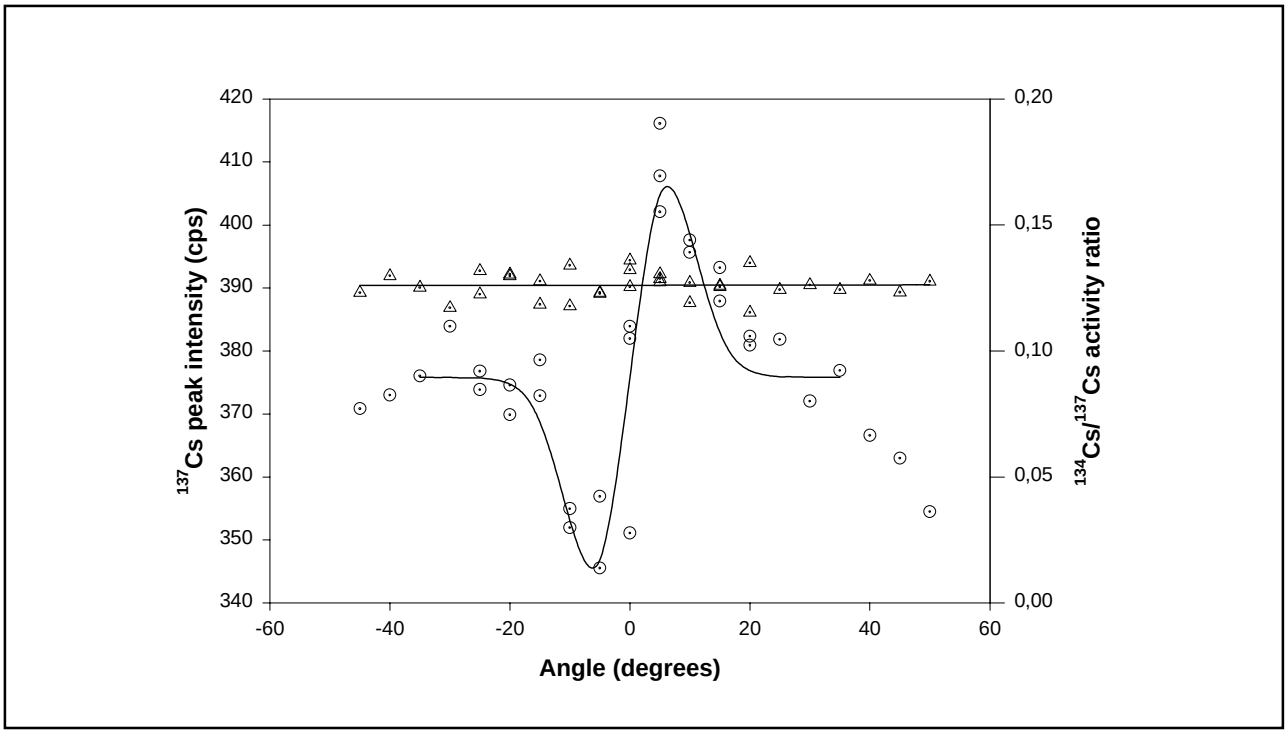

Figure 10. *Rotation scanning of assembly #12350. The left vertical axis represents the ^{137}Cs peak intensity (circles) and the right vertical axis the ^{134}Cs / ^{137}Cs activity ratio (triangles).*

5 SENSITIVITY TO HORIZONTAL POSITIONING

The A_{37} vs. horizontal distance to the CZT detector of assembly #12350 (x-coordinate) is investigated in Figure 11. The following linear curve was fitted to the data:

$$A_{37} = y_0 + a * x\,, \qquad (1)$$

where y_0 and a are the curve parameters. The slope a of the ^{137}Cs signal is about –10%/cm. During the subsequent measurements the water gap between an assembly and the entrance window of the CZT detector was kept as constant as possible (x = 0 cm). On the other hand, the Cs ratio seems to be almost independent of the distance as shown in Figure 11. The slope of the Cs ratio is –0.0022(±0.0014) cm^{-1}. The measured raw data are shown in Table A1.II in Annex 1.

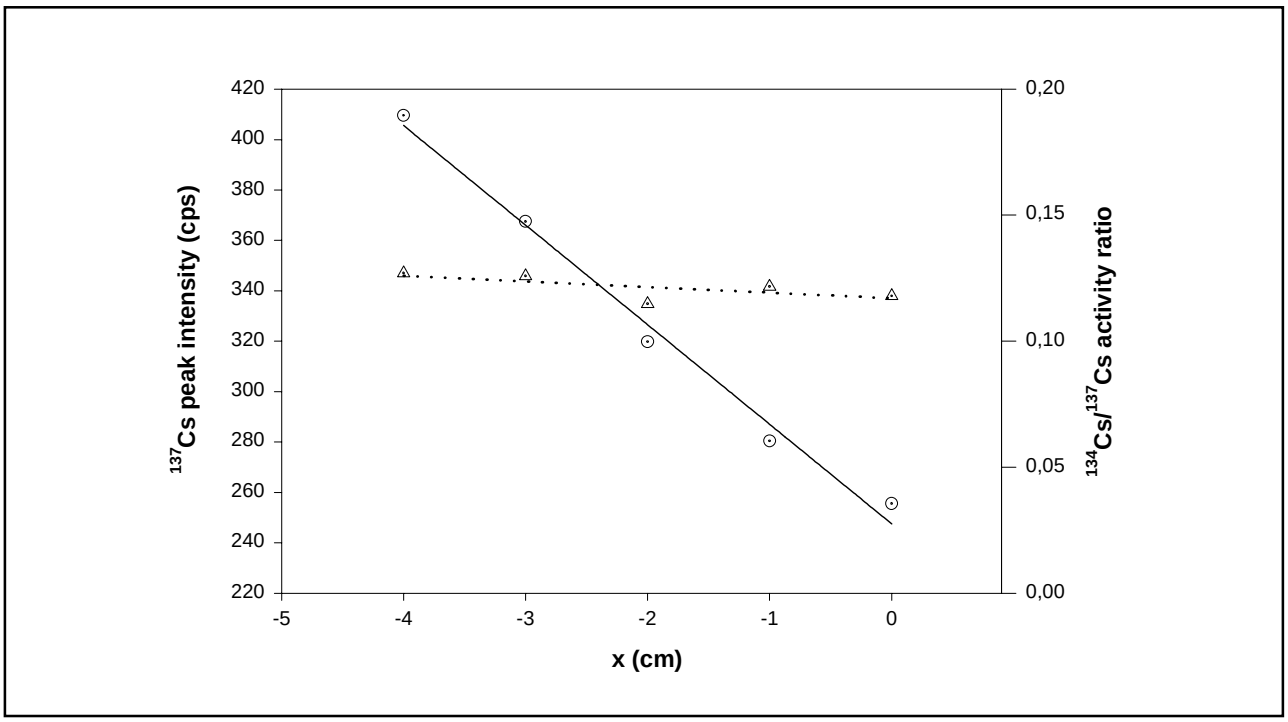

Figure 11. *Sensitivity of the gamma spectroscopic data to horizontal positioning. x=0 represents the standard measurement distance. x=–4 cm is the position closest to the CZT detector. The circles represent the ^{137}Cs signal, vertical scale on the left. The triangles display the ^{134}Cs / ^{137}Cs activity ratio, vertical scale on the right.*

6 MEASUREMENTS ON ONE VERTICAL LEVEL

All assemblies were measured at the same vertical level (z=5705) close to the mid-point of the assembly.

All measured data points have been taken into consideration in the following fits. Assembly #6124 was measured twice in the September measurements. The assembly #12323 was measured in both September and December campaigns to scale the measurement data of these campaigns. The measured raw data is shown in Tables A1.III and A1.IV in Annex 1.

The measurement data from all four sides were averaged and cooling time corrected to the discharge date: A_{37} and gross gamma data for ^{137}Cs and neutron data for ^{244}Cm.

6.1 Gamma measurements

Spent LWR fuel contains a variety of gamma emitting nuclides e.g. ^{137}Cs, ^{134}Cs, ^{154}Eu, ^{106}Ru/Rh and ^{144}Ce/Pr [11]. One measured gamma spectrum of the assembly #12323, is shown in Figure 12.

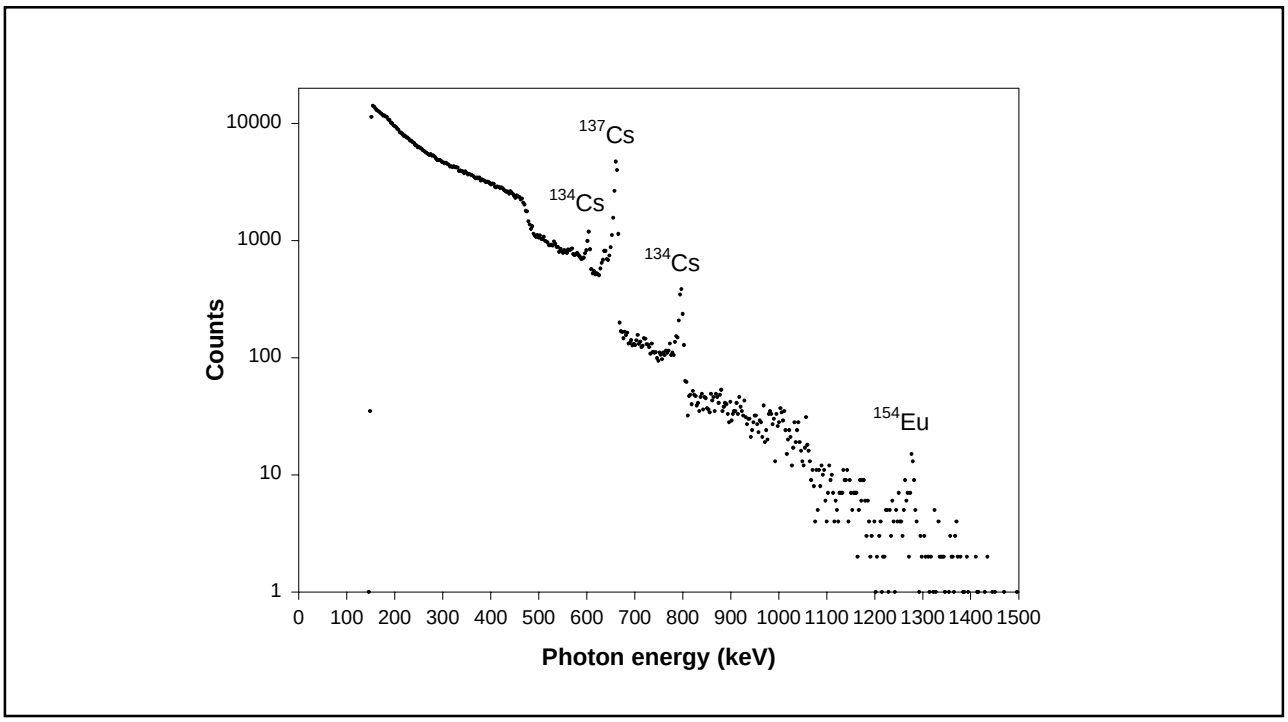

Figure 12. *Gamma spectrum of assembly #12323. Cooling time is about 9 years and burnup is 34 MWd/kgU.*

6.1.1 Correlation of ^{137}Cs signal to burnup

After a few years' cooling time ^{137}Cs is a dominant gamma emitter with the 662 keV gamma line and 30.07 years' half life. It has been shown that the amount of ^{137}Cs depends linearly on the burnup:

$$A_{37} = k * B, \quad (2)$$

where B denotes the average burnup of an assembly [12]. This curve is fitted to the measured ^{137}Cs peak intensity and shown in Figure 13.

The curve indicates that assemblies #10048 with burnup 28.282 MWd/kg, #12350 with burnup 35.37 MWd/kg, #0425 with burnup 39.039 MWd/kg and the ABB SVEA-64 assembly #16732 with burnup 35.21 MWd/kg seem to have a too high ^{137}Cs signal.

Tanskanen has studied the dependence of ^{137}Cs content of an assembly on enrichment, void fraction and amount of burnable absorber with several ORIGEN-S calculations. According to these calculations, all those dependencies were found very weak. [11]

The development of the ^{137}Cs activity for all measured fuel assemblies using the operator-declared data for individual assemblies was calculated using the PYVO program. The calculated ^{137}Cs activities have been scaled to correspond to the spectrometrically measured ^{137}Cs peak intensity or the measured gross gamma. The PYVO calculations for individual assemblies are shown by triangles in Figure 13.

Table IV. *Comparison of the regression parameters of the experimental and PYVO data for ^{137}Cs signal vs. burnup. R^2 denotes the correlation coefficient of the fit.*

	k cps/MWdkg^{-1}	σ_k	σ_k/k	R^2
Experimental	6.99	0.10	0.014	0.918
PYVO	7.01	0.01	0.002	0.999

The parameters of both fits are compared in Table IV. The consistency between the measurements and the PYVO calculations of individual assemblies is within 7.4% (σ, standard deviation) and the maximum deviation for an individual assembly is –2.1 (σ (assembly #10048).

In addition, the 90% prediction interval for the measured ^{137}Cs peak intensity vs. burnup curve is shown in Figure 13. This 90% confidence interval for the population describes the range where data values will fall at 90% probability for repeated measurements. This prediction interval is called as the *error corridor* in the remainder of this report. The width of this error corridor is about ±26% at the lowest burnup and about ±13% at the highest burnup measured.

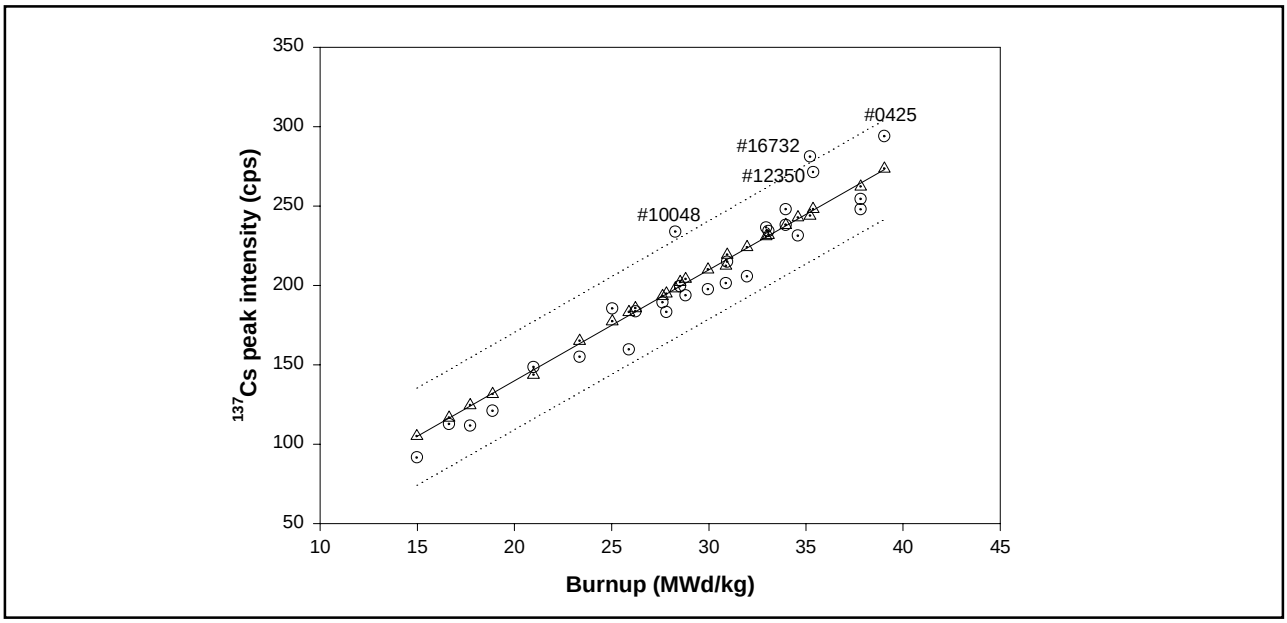

Figure 13. *Measured (circles) and calculated (triangles) ^{137}Cs intensity vs. burnup. The linear fit to the experimental data and the fit to the PYVO data coincide. Dotted lines describe the error corridor of the experimental data.*

Table V. *Emission probabilities and gamma emission energies of ^{137}Cs, ^{134}Cs and $^{106}Ru/Rh$. [14]*

$\varepsilon_{37,i}$	$E_{37,i}$ (keV)	$\varepsilon_{34,i}$	$E_{34,i}$ (keV)	$\varepsilon_{06,i}$	$E_{06,i}$ (keV)
0.851	661.660	0.9762	604.721	0.2040	511.84
		0.8553	795.864	0.0993	621.94
		0.1538	569.331	0.0156	1050.39
		0.0869	801.953		
		0.0835	563.246		

For cooling times greater than 1 year, the total gamma-ray activity is roughly proportional to the burnup [13].

$$G = k' * B, \tag{3}$$

where G denotes the gross gamma signal. However, some of the assemblies with cooling time <12 years and high burnup still contain ^{134}Cs, which disturbs the gross gamma curve leading to a large scatter of data points. Additional correction for ^{106}Ru/Rh has to be made to the gross gamma data of assemblies, which have only a few years' cooling time. In addition, the ^{137}Cs based cooling time correction would not be correct without first correcting for ^{134}Cs and ^{106}Ru/Rh.

6.1.2 Corrections applied to gross gamma signal

To investigate, whether the large scatter is caused by the ^{134}Cs activity, the ^{134}Cs activity was eliminated from the gross gamma data of both measurement campaigns. It was found that the ^{134}Cs correction leads to a significant improvement. The additional ^{106}Ru/Rh correction was made to the gross gamma data of the assembly #16732, which has the shortest cooling time of 3.6 years and a high burnup of 35.21 MWd/kg.

The basis of the ^{134}Cs and ^{106}Ru/Rh correction is that the gross gamma signal is assumed to be proportional to the total energy rate of the gamma emission of all isotopes. The emitted energy rates of each isotope can be calculated from the gamma spectroscopically determined activities. The main isotopes are ^{137}Cs, ^{134}Cs and ^{106}Ru/Rh in this case and the total gamma signal can be segregated into the components of each isotope:

$$G = G_{37} + G_{34} + G_{06}, \tag{4}$$

where G_{37}, G_{34} and G_{06} denote the gamma emission energy rates of ^{137}Cs, ^{134}Cs and ^{106}Ru/Rh respectively. Dependence of the detector efficiency on gamma energy is not taken into consideration. The gamma emission energy rates of ^{137}Cs, ^{134}Cs and ^{106}Ru/Rh are calculated according to the following equations:

$$G_{37} = A_{37} * \sum_i \left(\varepsilon_{37,i} * E_{37,i}\right) \tag{5}$$

$$G_{34} = A_{34} * \sum_i \left(\varepsilon_{34,i} * E_{34,i}\right) \tag{6}$$

$$G_{06} = A_{06} * \sum_i \left(\varepsilon_{06,i} * E_{06,i}\right) \tag{7}$$

where ε_i and E_i denote emission probabilities and gamma emission energies of ^{137}Cs, ^{134}Cs and ^{106}Ru/Rh for energy i. The emission probabilities and gamma emission energies are shown in **Table V**.

The ^{134}Cs and ^{106}Ru/Rh-corrected gross gamma, G_{37}, can be calculated using the equations (4), (5), (6) and (7) and Table V:

$$G_{37} = \frac{G}{1 + \frac{G_{34}}{G_{37}} + \frac{G_{06}}{G_{37}}} \tag{8}$$

leading to the final form

$$G_{37} = \frac{G}{1 + 2.620 * R_{34} + 0.324 * R_{06}}, \tag{9}$$

where R_{34} is the measured activity ratio of ^{134}Cs to ^{137}Cs and R_{06} is the measured activity ratio of ^{106}Ru/Rh to ^{137}Cs obtained from the gamma spectrometric data. The constants 2.620 and 0.324 come from the emissivities and energies of the isotopes. In the remainder of this report the *gross gamma* denotes the gross gamma signal corrected for ^{134}Cs and ^{106}Ru/Rh, whenever these isotopes contributed to the gross gamma signal.

^{106}Ru/Rh was identified only in the spectra of the assembly #16732, which has the shortest cooling time of 3.6 years. In very old assemblies the ^{134}Cs signal was no more visible either.

6.1.3 Correlation of gross gamma to burnup

A linear fit of the gross gamma data (G_{37}) vs. burnup according to

$$G_{37} = k'' * B \quad (10)$$

is shown in Figure 14.

In Figure 14 also the calculated ^{137}Cs activity (triangles) as scaled into the units of the experimental value together with its linear fit is displayed. The fitting parameters of both the experimental and the PYVO results are shown in Table VI.

The error corridor for the measured gross gamma vs. burnup curve is shown in Figure 14. Its width is about ±17% at the lowest burnup and about ±8% at the highest burnup.

Gross gamma correlates to the burnup significantly better than the gamma spectroscopically measured ^{137}Cs activity. For example, the assemblies #10048, #12350 and #0425 fit perfectly to the correlation curve when the ^{137}Cs emission is obtained from the gross gamma signal. This can be explaned by different sensitivity to positioning errors of these two methods. Mispositioning introduces a smaller error to gross gamma, equation(9), because of two reasons. The raw gross gamma is measured by the ionisation chambers placed along the x direction. This should damp the sensitivity to positioning error of an assembly in the x direction. On the other hand, positioning errors introduced to the gamma spectrometry data are cancelled in R_{34} and R_{06}. In fact, the activity ratio R_{34} is almost constant independent of both the x coordinate and the angle (see Figures 10 and 11). Instead, the ^{137}Cs signal itself is very sensitive to the positioning error in the x direction (see Figure 11).

Table VI. *Parameters of the gross gamma vs. burnup fit.*

	k''	$\sigma_{k''}$	$\sigma_{k''}/k''$	R^2
Experimental	20.45	0.18	0.009	0.963
PYVO	20.49	0.03	0.002	0.999

The assembly #13285 seems to emit too low gross gamma signal. This can be due to an off reactor cycle of this assembly. In other words, the assembly #13285 has effectively a longer cooling time than used in these calculations. On the other hand, the assembly #7289, which also has an off reactor cycle, fits perfectly to the correlation curve. Therefore this discrepancy of the assembly #13285 cannot be unambiguously attributed to its off-reactor cycle.

6.2 Neutron measurements

A dominant neutron emitter is curium for spent LWR fuel. At discharge, the neutron emission is

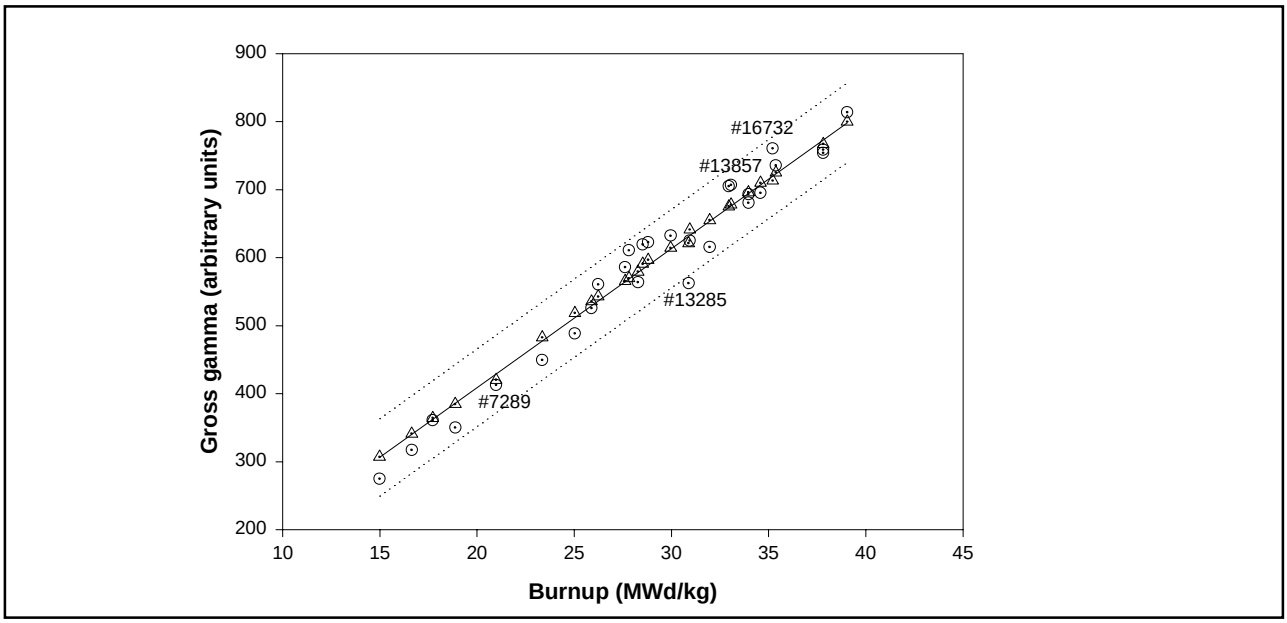

Figure 14. *Gross gamma signal vs. burnup. The circles represent the experimental points, the PYVO calculation results are shown as triangles. The linear fit to the experimental data and the fit to the PYVO data coincide. Dotted lines describe the error corridor of the experimental data.*

almost equally due to ^{242}Cm and ^{244}Cm. Owing to its short half-life, 163 days, ^{242}Cm rapidly decays after discharge. Instead, the half life of ^{244}Cm is 18.1 years. Thus, the neutron emission of spent LWR fuel, which has a cooling time longer than about 3 years, is mainly caused by spontaneous fission of ^{244}Cm. [11]

First it was checked whether there is any difference between the neutron counts of the Cd-wrapped fission chambers and the bare fission chambers. Correlation between these two neutron channels was perfectly linear. The correlation obtained in measurements performed in September is shown in Figure 15. The parameters received from the fits to the measured raw data of both measurement campaigns are shown in Table VII.

The zero cross-over value of the measurements performed in September deviates significantly from zero indicating a small misadjustment of either of the neutron channels. According to the correlation line there should have been about 7 cps in the Cd-wrapped channel as the bare channel indicates zero counts. Nevertheless, the measured background counts in both channels were zero during absence of a fuel assembly. One possible explanation is slight gamma sensitivity of the Cd-wrapped channel. As the signals in both channels are otherwise equivalent, the bare fission chamber signal is used in all subsequent considerations.

Table VII. *Linear correlation parameters between the neutron counts of the bare and Cd-wrapped fission chambers.*

	September		December	
	Value	σ	Value	σ
Slope	1.767	0.008	1.545	0.013
Zero cross-over	-13.1	1.8	2.7	3.2
R^2	0.9998		0.9994	

According to Würz [15], the assembly-averaged primary ^{244}Cm neutron source at discharge of spent LWR fuel, with burnup higher than 18 MWd/kgU, can be described using the following equation

$$S_p^0 = a * B^b, \tag{11}$$

where S_p^0 denotes the primary ^{244}Cm neutron source at discharge
B denotes the discharge burnup
a and b denote fuel type dependent constants.

6.2.1 Corrections applied to neutron signal

Assemblies with low initial enrichment need higher neutron fluence to yield the same burnup as assemblies with higher enrichment. Higher neutron fluence means higher concentration of ac-

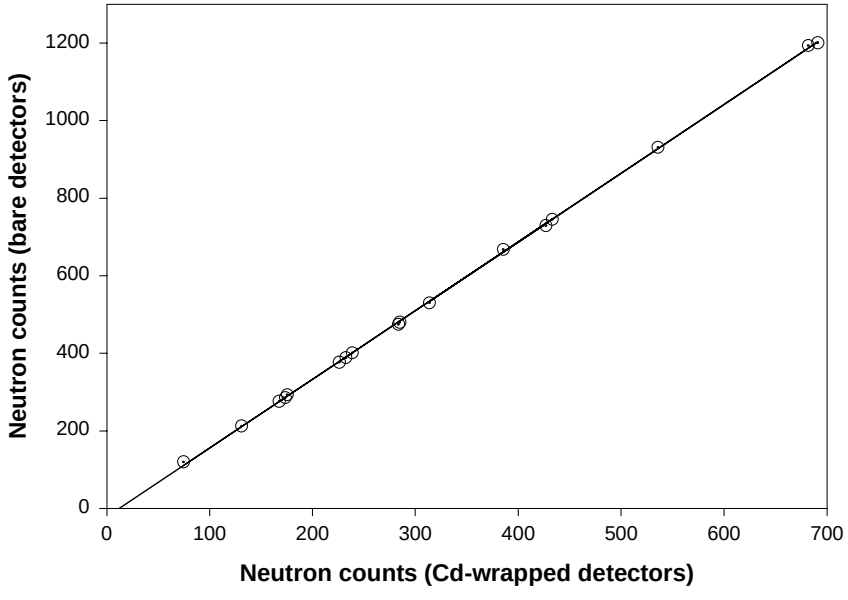

Figure 15. *Correlation between the bare and Cd-wrapped fission chambers.*

Table VIII. *Parameters of the ^{244}Cm neutron yield vs. initial enrichment fits with different burnup values.*

Burnup (MWd/kg)	s	σ_s	r	σ_r	R^2
15	$3.3663 \cdot 10^7$	$0.2643 \cdot 10^7$	0.9774	0.0394	0.9945
20	$1.0148 \cdot 10^8$	$0.0632 \cdot 10^8$	0.8694	0.0304	0.9955
25	$2.2148 \cdot 10^8$	$0.0998 \cdot 10^8$	0.7769	0.0212	0.9971
30	$3.9399 \cdot 10^8$	$0.1231 \cdot 10^8$	0.6961	0.0143	0.9983
35	$6.1714 \cdot 10^8$	$0.1273 \cdot 10^8$	0.6250	0.0092	0.9991
40	$8.7467 \cdot 10^8$	$0.0927 \cdot 10^8$	0.5590	0.0046	0.9997

tinides and thus higher neutron emission. [12] In other words, for the same burnup, lower enrichment should give a higher ^{244}Cm neutron source. The initial operator declared enrichment of the measured assemblies is given in Table I.

The type of the assemblies #16732 and #13857 is ABB SVEA-64 and the type of the assemblies #0425 and #0104 is Siemens 9×9-1. All other assemblies are of type ABB 8×8-1.

The enrichment dependence of the ^{244}Cm neutron source at discharge was investigated with help of ORIGEN-S calculations. The enrichment varied from 1.6% to 4.4% and the burnup from 15 MWd/kg to 40 MWd/kg. The fuel assembly model was a common ABB 8×8-1 BWR fuel without rods containing burnable absorber. The average power of the bundle was set at 4.5 MW and the desired burnup was achieved by adjusting the time that the bundle spent in the reactor.

The calculations were performed using void fraction values of the coolant 0, 0.2, 0.4 and 0.5 inside an assembly and 0 in the channel. The ORIGEN-S calculation results for ^{244}Cm neutron source with void fraction 0 and burnup 20, 30 and 40 MWd/kg are found in ref. [11]. The results of the calculation performed with the void fraction 0.5 corresponding to the moderator density 0.392 g/cm^3 were chosen for use in the enrichment correction, because this void fraction value corresponds best to the real average situation in a BWR reactor. The calculated ^{244}Cm neutron sources at discharge are shown in Table A2.I in Annex 2.

To obtain a recipe for the enrichment correction the ^{244}Cm neutron source was correlated to the initial enrichment while the burnup and void fraction were kept constant. The ^{244}Cm neutron source was correlated to the initial enrichment according to the equation

$$N_O = s * e^{-r*IE} \tag{12}$$

where N_O denotes the ^{244}Cm neutron source at discharge
IE denotes the initial enrichment and
s and r denote burnup and void fraction dependent parameters received from the fit.

The parameters received from the fits corresponding to different burnup values and the void fraction 0.5 are shown in Table VIII. Correlation curves with six different burnup values are shown in a semi-logarithmic scale in Figure 16.

Utilizing Table VIII, the parameter r was correlated to the burnup according to the equation

$$r = t_1 + t_2 * B \tag{13}$$

where t_1 and t_2 denote void fraction dependent paremeters received from the fit and
B denotes the discharge burnup.

When the void fraction is 0.5, the values of parameters received from the fit are t_1 = (1.2073 ± 0.0224)%$^{-1}$, t_2 = (–0.0166 ± 0.0008) (%*MWd/kg) $^{-1}$ and R^2 = 0.9913 (Figure 17). In fact, the linearity improves as the void fraction decreases. When considering the measurement data, fitting to the first degree correlation curve is sufficient.

The enrichment correction equation corresponding to the void fraction value of 0.5 can be calculated using equations (12) and (13):

$$N_R = N * e^{(1.2073 - 0.0166*B)*(IE - IE_R)} \tag{14}$$

where N_R denotes the ^{244}Cm neutron countrate of an assembly at discharge as corrected to the reference enrichment,
N denotes the measured ^{244}Cm neutron count rate of an assembly as corrected to the discharge date,
IE_R denotes the reference enrichment, which was chosen to be 2.95%,

IE denotes the operator declared initial enrichment of the assembly and
B denotes the discharge burnup.

The measured fission chamber count rates have been corrected for the enrichment variation, the share of ^{244}Cm neutrons and the decay of ^{244}Cm. They have been correlated to the burnup, the measured ^{137}Cs signal and the gross gamma signal in Figures 18–24. The share of ^{244}Cm neutrons of the total neutron emission has been obtained from calculations with PYVO and it varied from 0.76 to 0.97. The calculation of ^{244}Cm share of the total neutron counts was checked with ORIGEN-S. The results received from these two codes were equal. E.g. for the assembly #12323 the share of ^{244}Cm neutrons was 0.962 as calculated with PYVO and 0.963 as calculated with Origen-S.

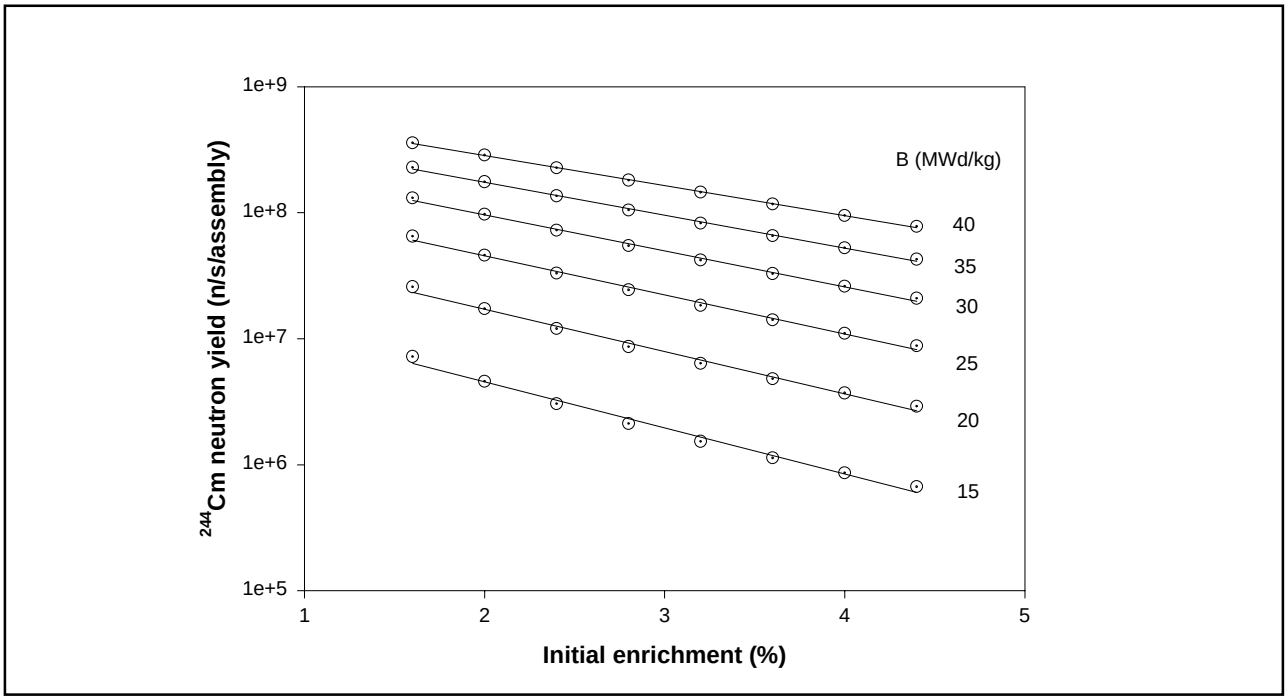

Figure 16. *Calculated ^{244}Cm neutron yield vs. initial enrichment. Void fraction is 0.5 and burnup is varied from 15 MWd/kg to 40 MWd/kg.*

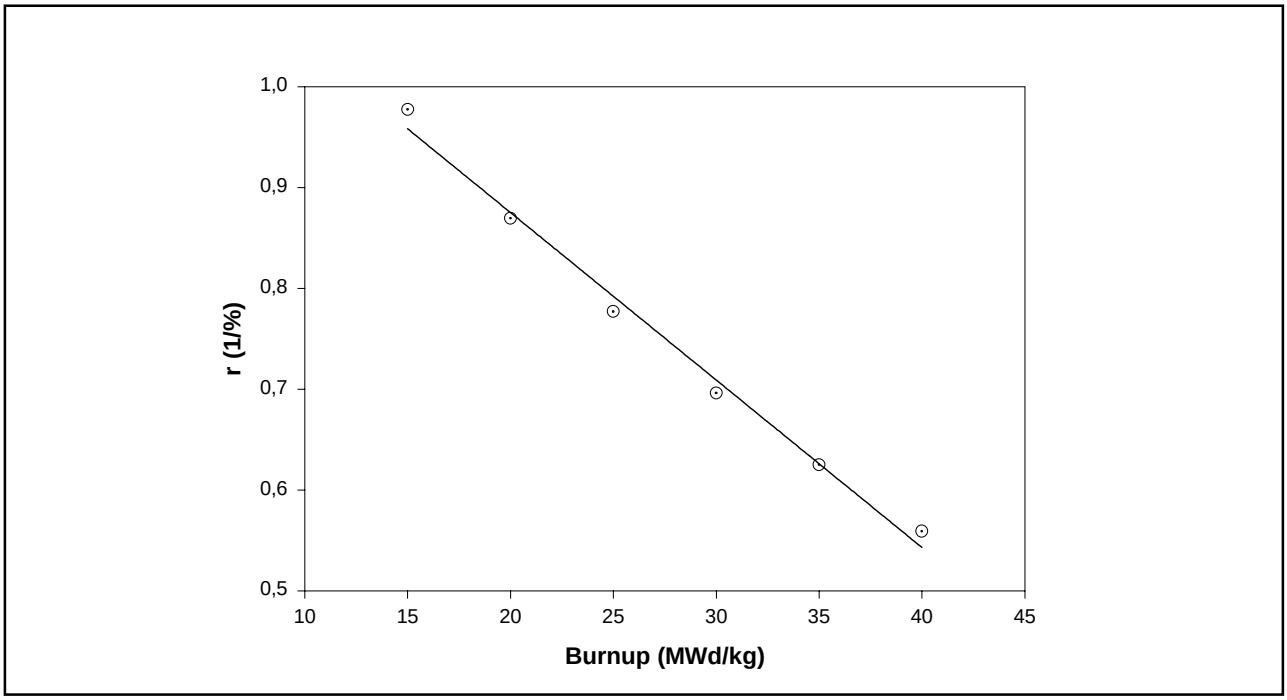

Figure 17. *Coefficient r vs. burnup at void fraction 0.5.*

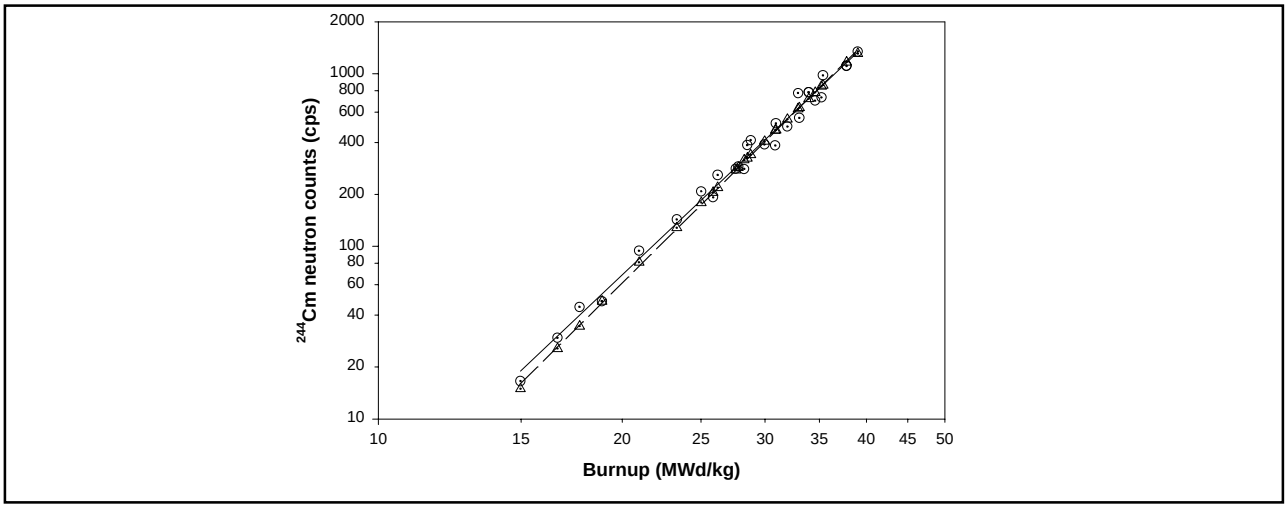

Figure 18. *^{244}Cm neutrons vs. burnup. The circles represent the experimental values and the triangles represent the PYVO data. Solid line represents the fit to the experimental results and the dashed line the fit to the PYVO results.*

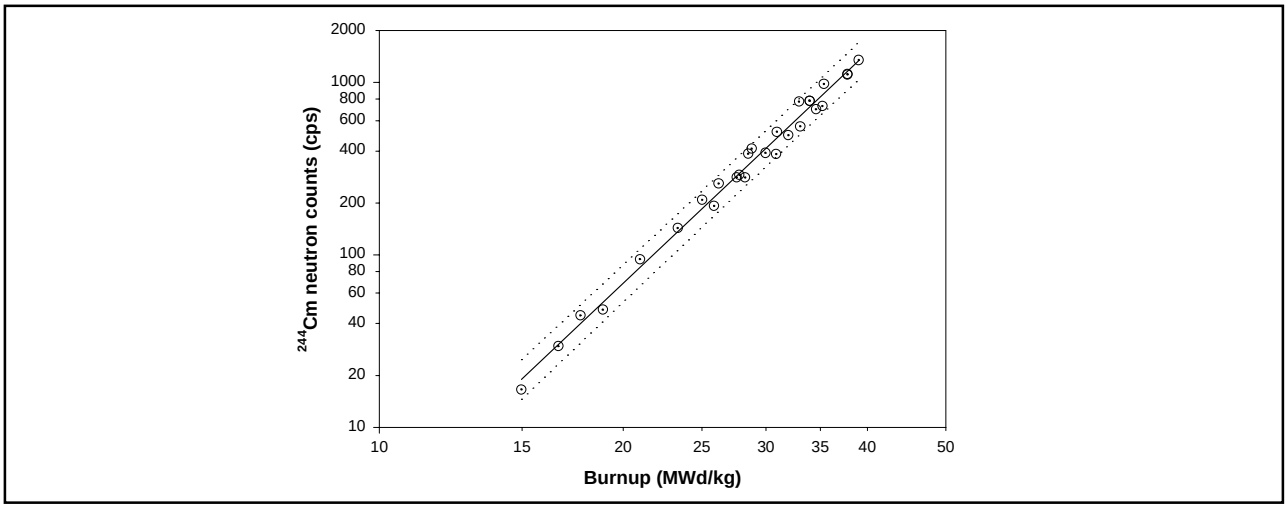

Figure 19. *^{244}Cm neutrons vs. burnup. Dotted lines limit the error corridor.*

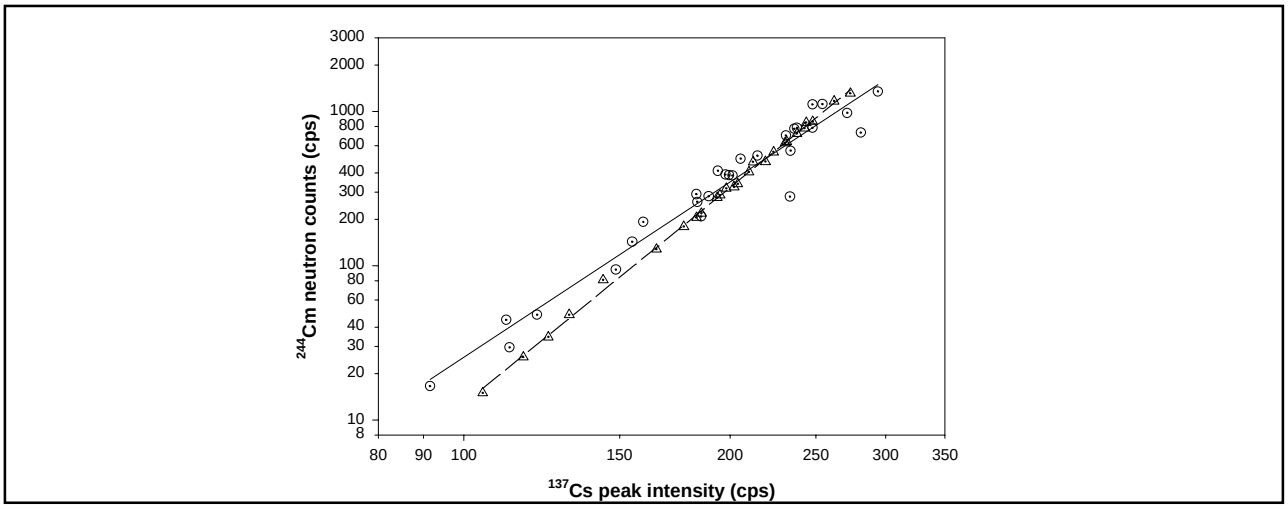

Figure 20. *^{244}Cm neutrons vs. the ^{137}Cs peak intensity. The circles represent the experimental values and the triangles represent PYVO data. Solid line represents the fit to the experimental results and the dashed line is the fit to the PYVO calculation results.*

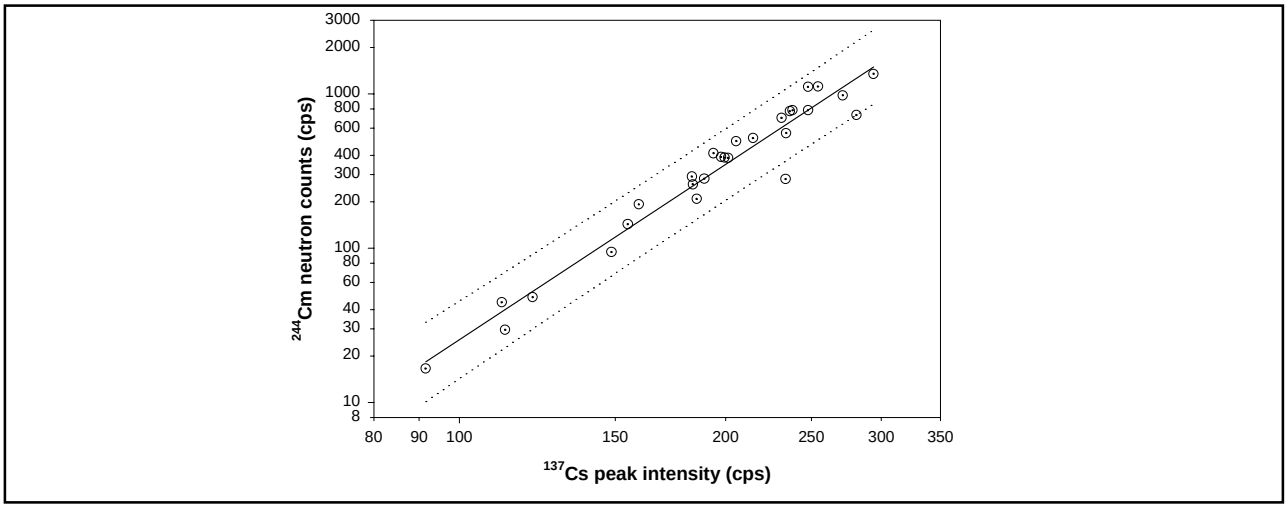

Figure 21. *^{244}Cm neutrons vs. ^{137}Cs peak intensity. Dotted lines describe the error corridor.*

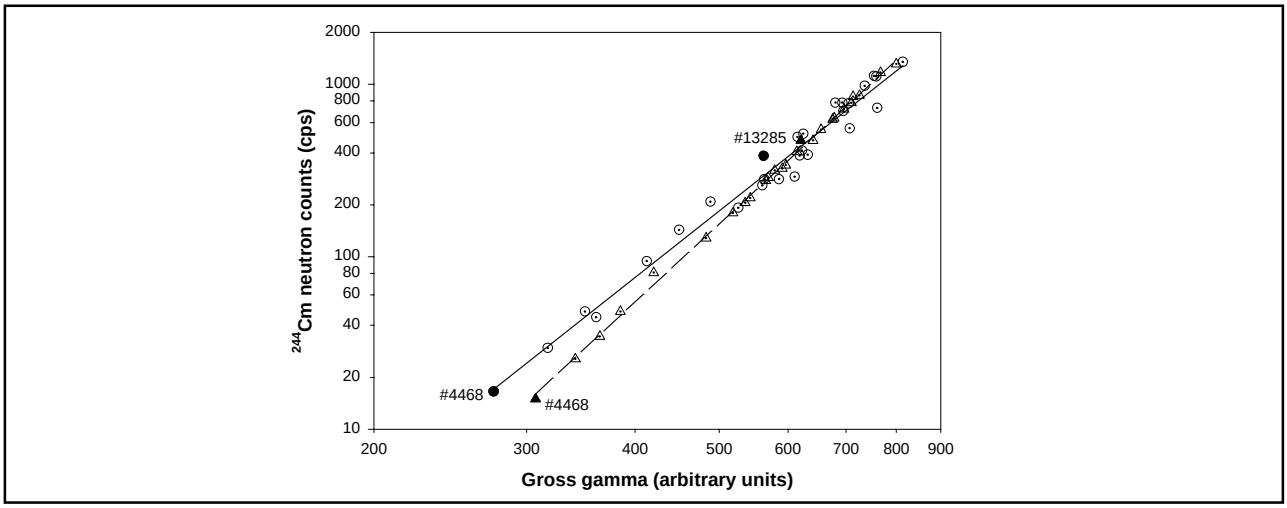

Figure 22. *^{244}Cm neutrons vs. the gross gamma signal. The experimental points are shown in circles and the PYVO calculations for individual assemblies in triangles. The solid line represents the fit to the experimental points and the dashed line shows the fit to the PYVO calculations. Filled circles and triangles represent the assemblies #4468 and #13285.*

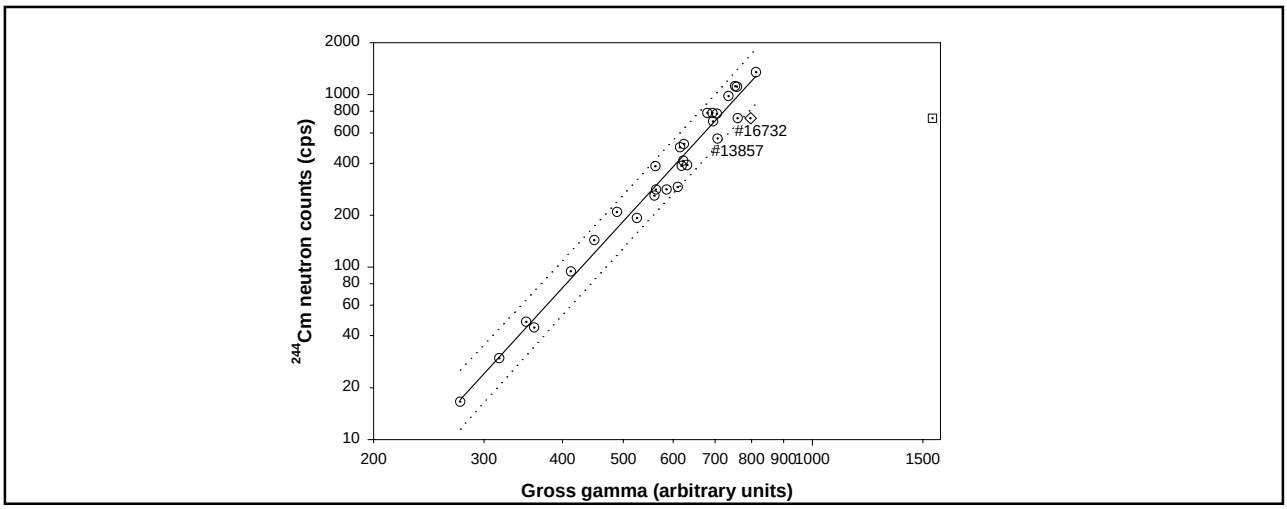

Figure 23. *^{244}Cm neutrons vs. gross gamma signal. Dotted lines describe the error corridor. The square represents the case when only the cooling time correction has been applied to the measured gross gamma signal of the assembly #16732. The diamond represents the case when the gross gamma signal of the assembly #16732 has been corrected for ^{134}Cs. The circle to the left of the diamond is the data point of the assembly #16732, when the gross gamma signal has been corrected for both ^{134}Cs and ^{106}Ru/Rh.*

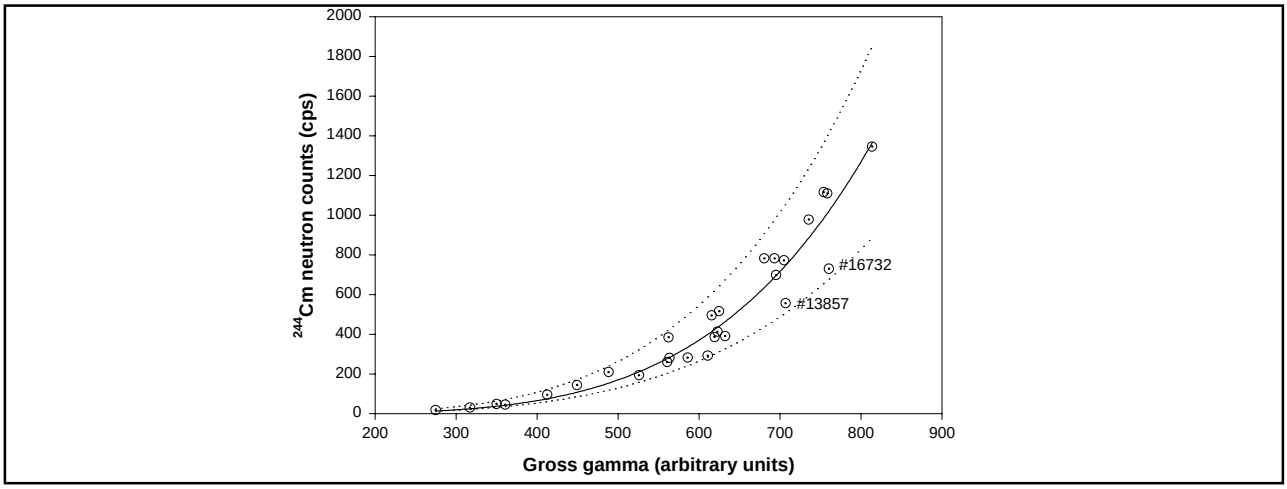

Figure 24. *^{244}Cm neutrons vs. the gross gamma signal. Dotted lines describe the error corridor.*

Table IX. *Neutrons vs. burnup, parameters of equation (15). UL and LL indicate the parameters of the upper and lower limit, respectively, of the error corridor, shown by dotted lines in Figure 19.*

	Enrichment correction	α	σ_α	b_α	σ_b	R^2
PYVO	yes	–4.27	0.03	4.65	0.02	1.000
Experimental	yes	–3.95	0.13	4.44	0.09	0.990
UL	yes	–3.82		4.43		
LL	yes	–4.08		4.46		
Experimental	no	–2.10	0.22	3.22	0.15	0.946

6.2.2 Correlation of neutron signal to burnup

Neutrons were correlated to burnup according to equation (15):

$$\log_{10}(N) = \alpha + b * \log_{10}(B), \quad (15)$$

where N is the measured neutron count rate. α and b are the parameters received from the fit. The results are shown in Table IX. The fit of the experimental results coincide within the statistical accuracy to the corresponding fit of the PYVO calculations.

The fit is much worse, if the enrichment correction is not applied. Furthermore, the fitting parameters deviate significantly from the results calculated with PYVO. The results calculated using data without the enrichment correction are also shown in Table IX.

The value of b in equations (11) and (15) has been calculated by Anttila and Tanskanen. According to Anttila's ORIGEN-2 calculations, b varies from 4.5 to 4.8 [16]. Tanskanen has determined the value of b by a series of ORIGEN-S calculations, which imply that b = 4.67 (when moderator density = 0.5 g/cm^3 and initial enrichment = 3.0%) and b = 5.03 (when moderator density = 0.752 g/cm^3 and initial enrichment = 3.0%) [11]. The values of b obtained from the measurement results (Table IX) correspond quite well to these calculated values.

The error corridor for the measured ^{244}Cm neutron counts vs. burnup curve is shown in Figure 19. The parameters of the upper and lower limiting curves of the error corridor are also given in Table IX. The width of this error corridor is about ±4.6%.

6.2.3 Correlation of neutron signal to gamma signal

Neutrons were correlated to the measured ^{137}Cs peak intensity and the gross gamma signal according to the equations:

$$\log_{10}(N) = \alpha' + b' * \log_{10}(A_{37}), \quad (16)$$

$$\log_{10}(N) = \alpha'' + b'' * \log_{10}(G_{37}), \quad (17)$$

where α', b', α'' and b'' are parameters received from the fit. Enrichment correction has been applied to the neutron data of these fits. The results are shown in Tables X and XI and plotted in Figu-

Table X. *Neutrons vs. the ^{137}Cs peak intensity. UL and LL as in Table IX.*

	a'	$\sigma_{a'}$	b'	$\sigma_{b'}$	R^2
PYVO	–8.21	0.09	4.66	0.04	0.998
Experimental	–6.15	0.39	3.78	0.17	0.951
UL	–5.84		3.75		
LL	–6.45		3.80		

Table XI. *Neutrons vs. gross gamma. UL and LL as in Table IX.*

	a''	$\sigma_{a''}$	b''	$\sigma_{b''}$	R^2
PYVO	–10.38	0.11	4.66	0.04	0.998
Experimental	–8.48	0.32	3.98	0.12	0.978
UL	–8.26		3.96		
LL	–8.70		4.00		

res 20–24.

Neutrons correlate better to gross gamma than to the measured ^{137}Cs activity. Again, this is probably due to the smaller position error of the gross gamma than the ^{137}Cs signal as described in the previous section.

When compared with the PYVO calculations, the agreement seems to be incomplete. However, the correspondence between the measured and PYVO fits is better for the gross gamma than for the ^{137}Cs peak intensity. The measured data points deviate from the calculated ones especially when the assemblies with low burnup are concerned. This may be due to the feature of the PYVO program, that it is optimized for the high burnup values [17].

The slope of the PYVO curves is independent on whether the calculated ^{244}Cm neutrons are correlated to the calculated ^{137}Cs intensity or the operator declared burnup. The slope of the measured ^{244}Cm neutron counts vs. gross gamma curve deviates more from the corresponding PYVO value than the slope of the measured ^{244}Cm neutron counts vs. burnup curve. The reason to this may be the scatter of the measured data points in the gross gamma vs. burnup curve.

The error corridor is shown in Figures 21, 23 and 24. The error corridor width of the the ^{244}Cm neutron counts vs. gross gamma curve is about ±6.8%. Concerning the ^{244}Cm neutron counts vs. ^{137}Cs peak intensity curve, the corresponding width is ±10.2%. The error corridor is ±4.6% when ^{244}Cm neutron counts are correlated to the declared burnup.

The agreement of individual assemblies in Figure 22 between the measured and calculated results is in the gross gamma scale within 5.2% (σ, standard deviation) and in the neutron scale 12.3% (σ, standard deviation). The gross gamma signal of assemblies #13285 and #4468 deviate significantly (more than 2σ) from their PYVO-calculated values. The deviation of assembly #13285 is 2.01σ in the gross gamma signal and 1.85σ in the neutron signal. The deviation of assembly #4468 is 2.27σ in the gross gamma signal and -0.78σ in the neutron signal.

All measured data points are inside the error corridor when neutrons are correlated to the gross gamma. This indicates that a single calibration curve could be used for assemblies of type ABB 8×8-1, Siemens 9×9-1 and ABB SVEA-64 (Figure 23 and Figure 24). The gross gamma signal of the assembly #16732, which has the shortest cooling time, was corrected also for ^{106}Ru/Rh. The effect of ^{134}Cs and ^{106}Ru/Rh correction to the gross gamma signal is demonstrated in Figure 23.

6.3 Importance of averaging the measurement data

^{244}Cm neutron counts were correlated to the gross gamma according to equation (17) without averaging the data over four sides of assemblies (Figure 25). The corresponding corrections to the measurement data as mentioned in sections 6.1 and 6.2 have been made to the gross gamma data and neutron data. The results received from the fit are shown in Table XII. The error corridor width is about ±7.2%, whereas for the averaged data it was ±6.8%. Averaging of four equivalent measurements has only a small effect to the error corridor width. This indicates that the width of the error corridor is primarily determined by real variation of the factors affecting the gamma and neutron emission of different assemblies (irradiation history, local conditions during irradiation etc.) rather than by random factors affecting the accuracy of an individual measurement (positioning accuracy, counting statistics etc.). In order to average real asymmetries due to irradiation history, measuring the neutron counts and gross gamma from all four sides of the assembly may be important. This would require two measurements with 90° rotation per assembly.

The azimuthal anisotropy of A_{37} seems to vary from assembly to assembly ranging from about

±1.1% to ±18.7%, when all measurements are taken into consideration.

6.4 Comparison of MMCA and DART, CsRatio and SAMPO

During the measurements of the September campaign one measurement spectrum was taken with both the DART and the MMCA analyser for each assembly at one azimuthal position. The spectrum from the MMCA was evaluated with the CsRatio and the spectrum from the DART was evaluated with the SAMPO. The results are shown in Figure 26. There is a systematic difference in the peak areas, which is not much of concern since the measurements are relative, not absolute. The standard deviation of all ratios is ±2.5%. The errors of the peak areas given by both programs range between 1 and 2%. Thus, it can be concluded that both MCAs and both analyser programmes provide similar results, but seem to underestimate the errors somewhat.

Table XII. *^{244}Cm neutrons vs. gross gamma without averaging over four sides of an assembly. UL and LL as in Table IX.*

	a''	$\sigma_{a''}$	b''	$\sigma_{b''}$	R^2
Experimental	–8.39	0.18	3.95	0.07	0.970
UL	–8.20		3.94		
LL	–8.58		3.96		

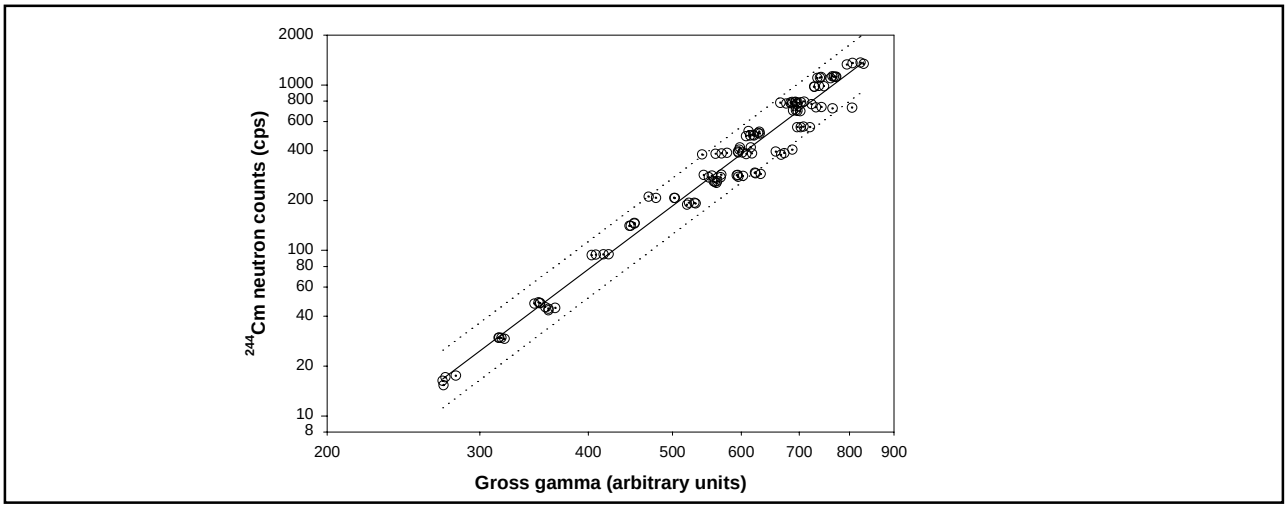

Figure 25. *^{244}Cm neutrons vs. gross gamma signal without averaging over four sides of an assembly. Dotted lines describe the error corridor.*

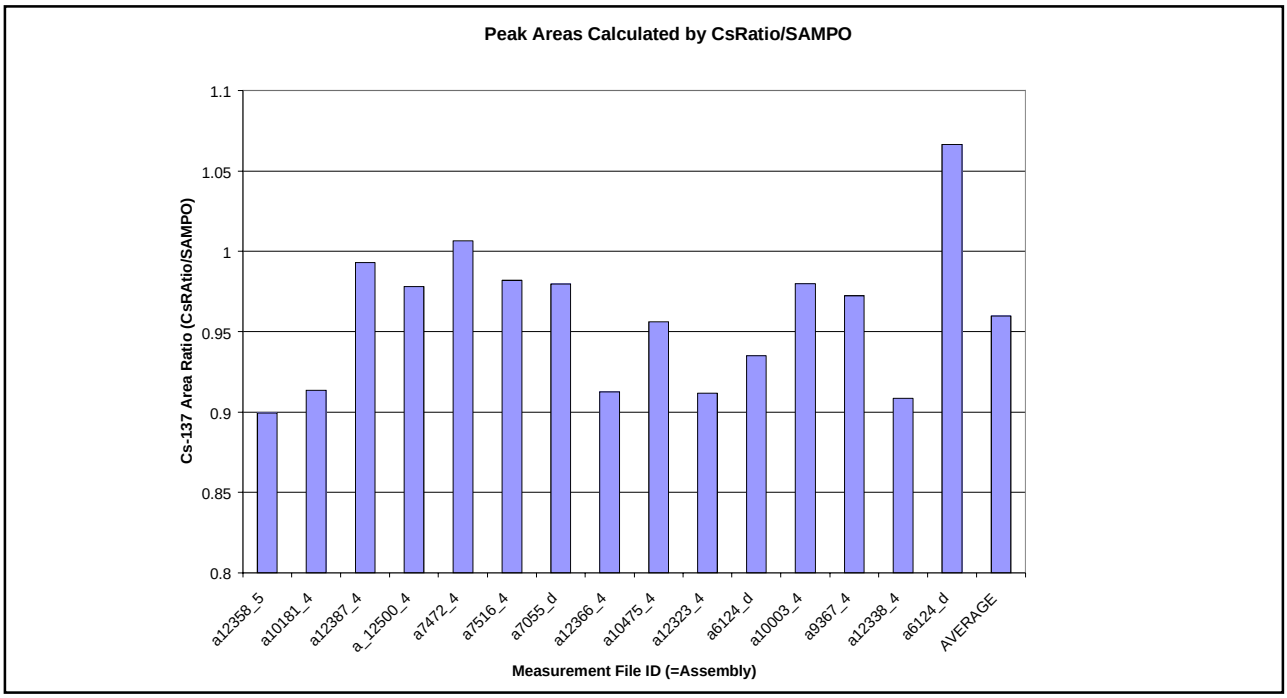

Figure 26. *Ratio of the peak areas calculated by CsRatio and SAMPO.*

7 AXIAL SCANNING

The measured axial scanning results of the assembly #6124 are shown in Figures 27 and 28. The neutron source distribution and burnup distribution of this assembly have been calculated by Tanskanen [11]. The results of these calculations are also shown in Figures 27 and 28. The measured axial scanning results of the assemblies #7055 and #12323 are shown in Figures 29–32. The assembly #7055 was scanned axially in November 1998 measurements, too. The raw data of these measurements are shown in Tables A1.V and A1.VI in Annex 1.

Figures 28, 30 and 32 show that not only the integral neutron emission but also the axial distribution of the neutron emission is independent on whether the measurement is taken with bare or Cd-wrapped fission chambers. The agreement between the measured and calculated distributions seems to be good. In the upper part of the assembly the gross gamma seems to follow better the calculated distribution than the measured ^{137}Cs peak intensity, see Figure 27. It is to be notified that the measured axial distributions of the assemblies #6124, #7055 and #12323 seem to be different from each other, see Figures 33 and 34. This stresses for the importance of choosing a correct measurement height in order to get consistent data from different assemblies. This question is further considered in the next section.

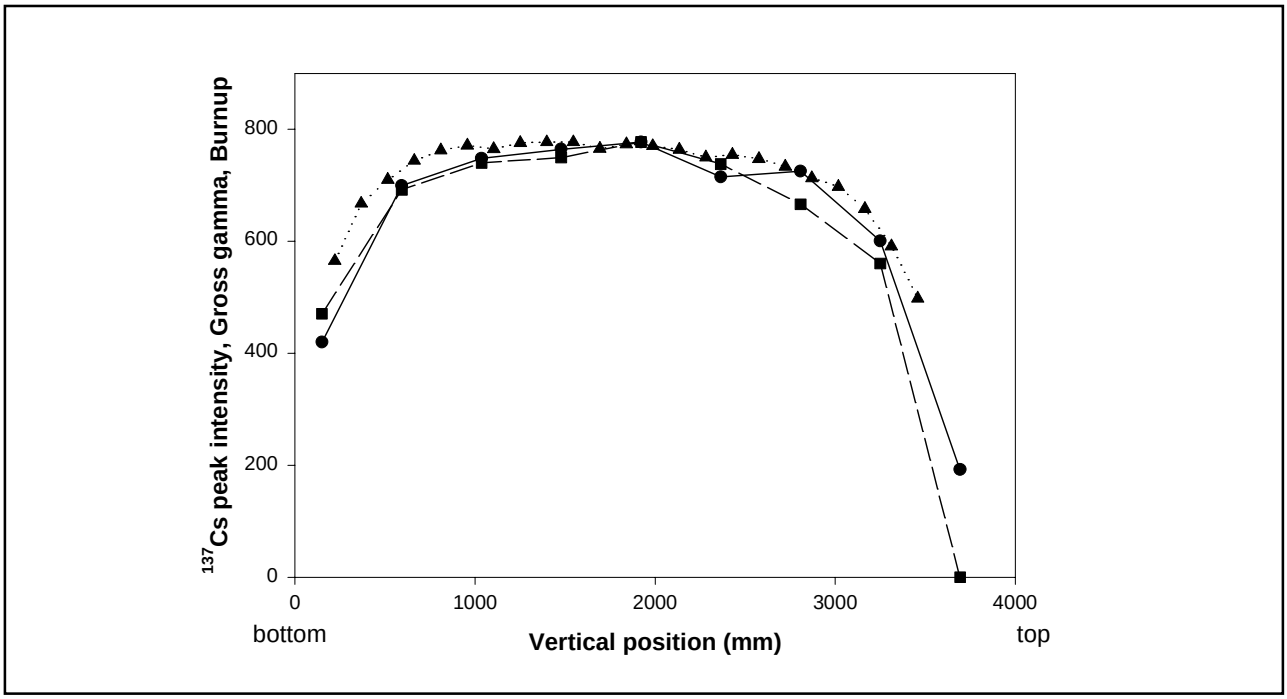

Figure 27. *Axial scanning of the assembly #6124. Triangles and dotted line represent the calculated burnup [11], squares and dashed line represent the measured ^{137}Cs peak intensity and circles and solid line represent the measured gross gamma signal.*

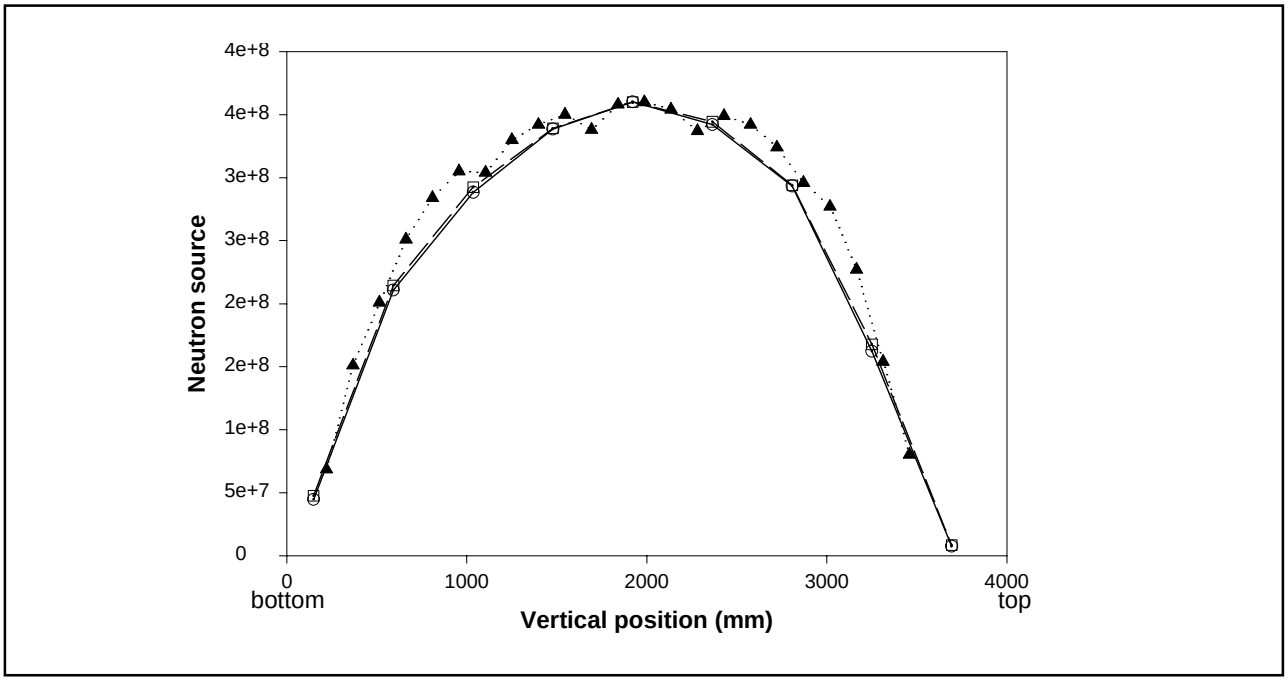

Figure 28. *Axial scanning of assembly #6124. Triangles and dotted line represent the calculated neutron source [11], squares and dashed line represent the measured neutron intensity from Cd-wrapped fission chambers and circles and solid line represent the measured neutron intensity from bare fission chambers.*

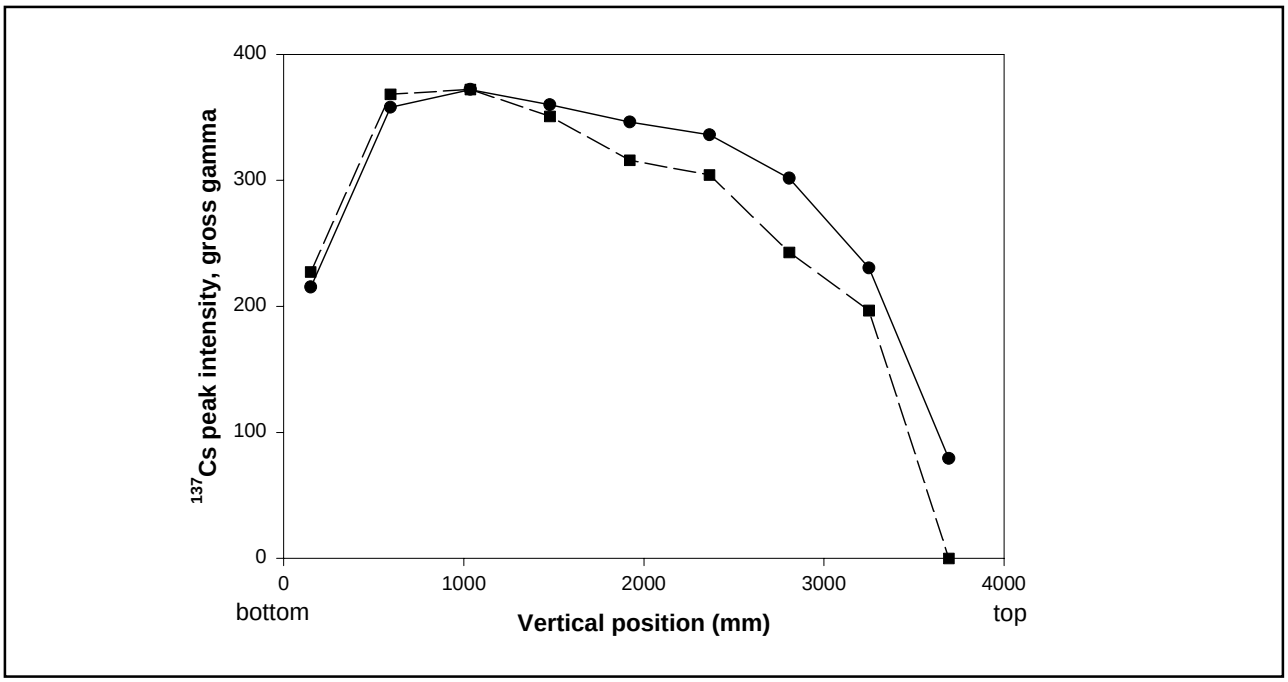

Figure 29. *Axial scanning of assembly #7055. Squares and dashed line represent the measured ^{137}Cs peak intensity whereas circles and solid line represent the measured gross gamma signal.*

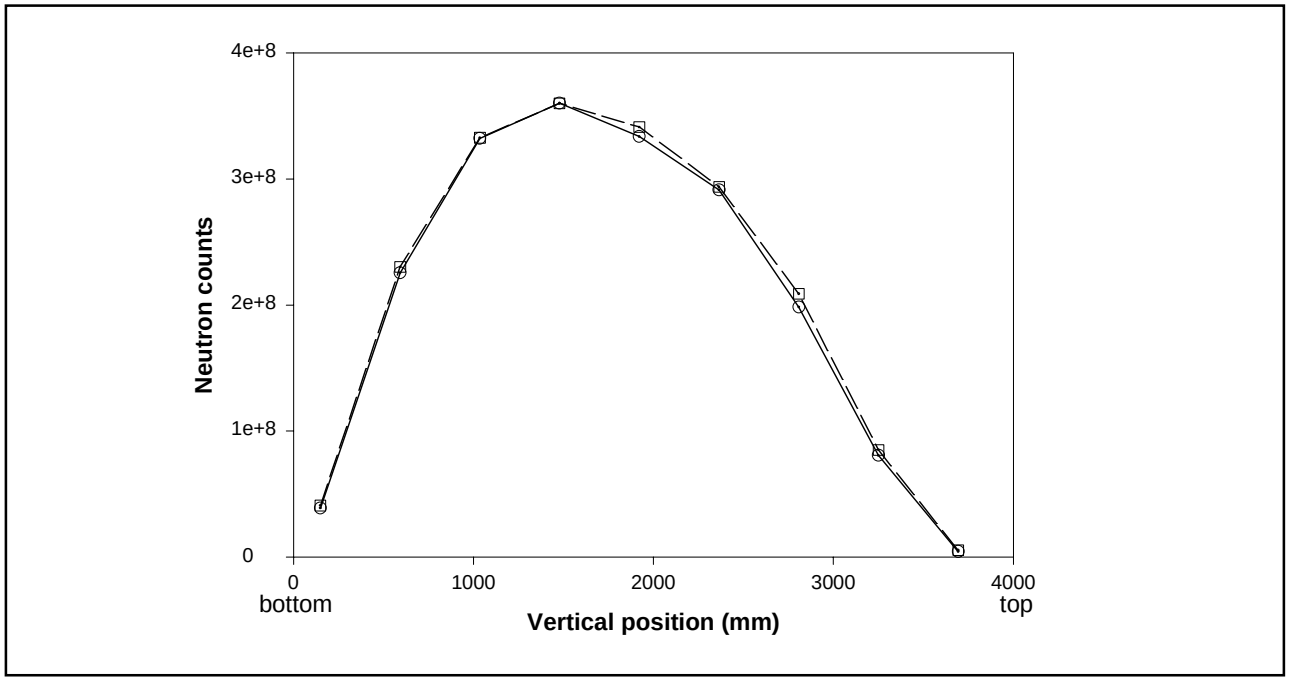

Figure 30. *Axial scanning of assembly #7055. Squares and dashed line represent the measured neutron intensity from Cd-wrapped fission chambers whereas circles and solid line represent the measured neutron intensity from bare fission chambers.*

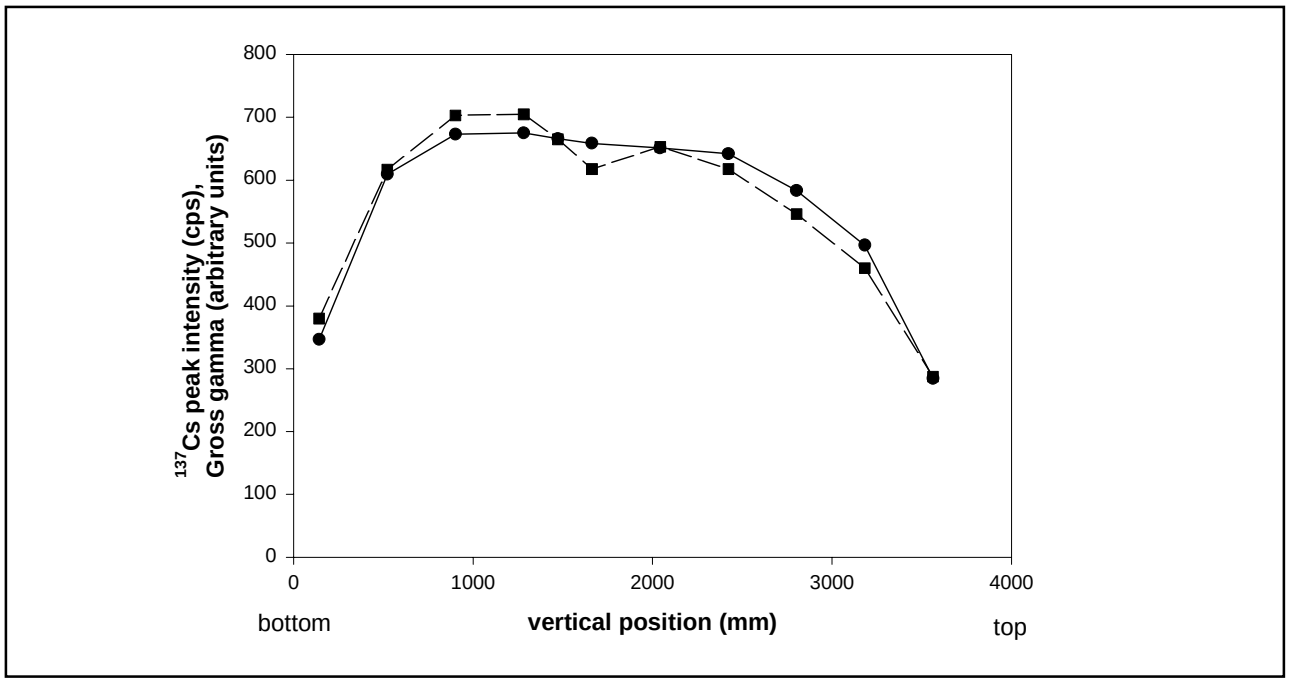

Figure 31. *Axial scanning of assembly #12323. Squares and dashed line represent the measured ^{137}Cs peak intensity whereas circles and solid line represent the measured gross gamma signal.*

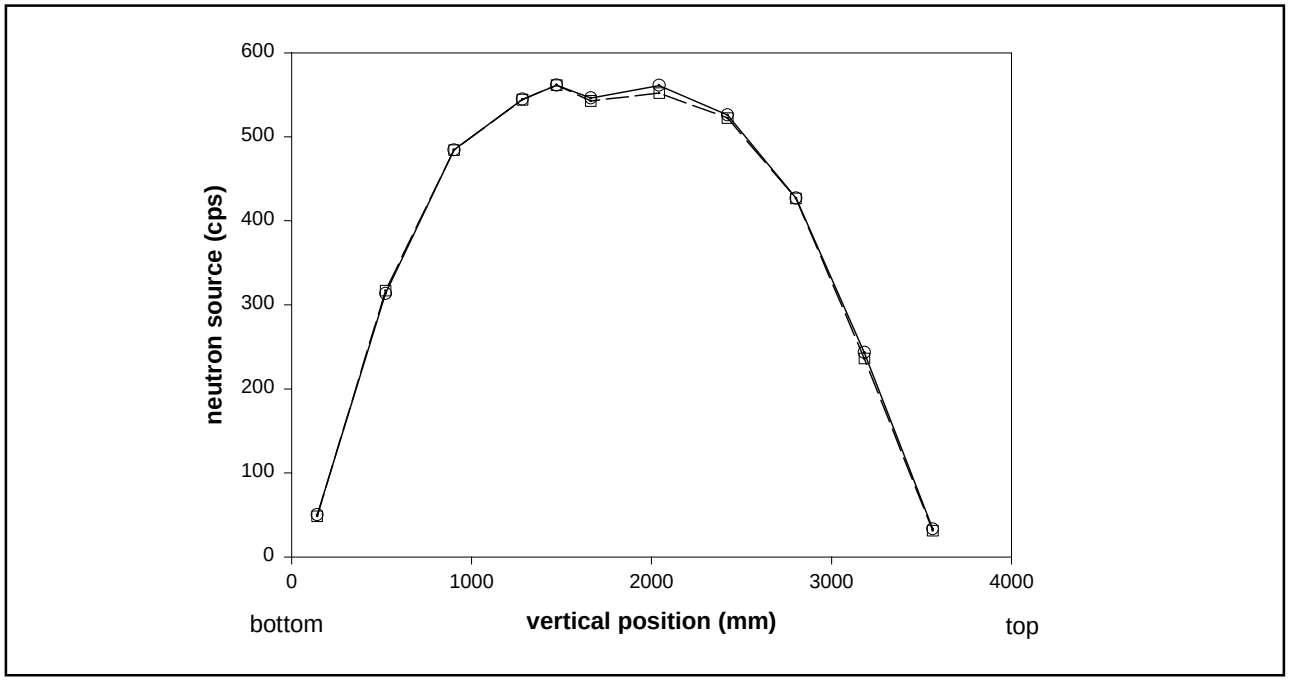

Figure 32. *Axial scanning of assembly #12323. Squares and dashed line represent the measured neutron intensity from Cd-wrapped fission chambers whereas circles and solid line represent the measured neutron intensity from bare fission chambers.*

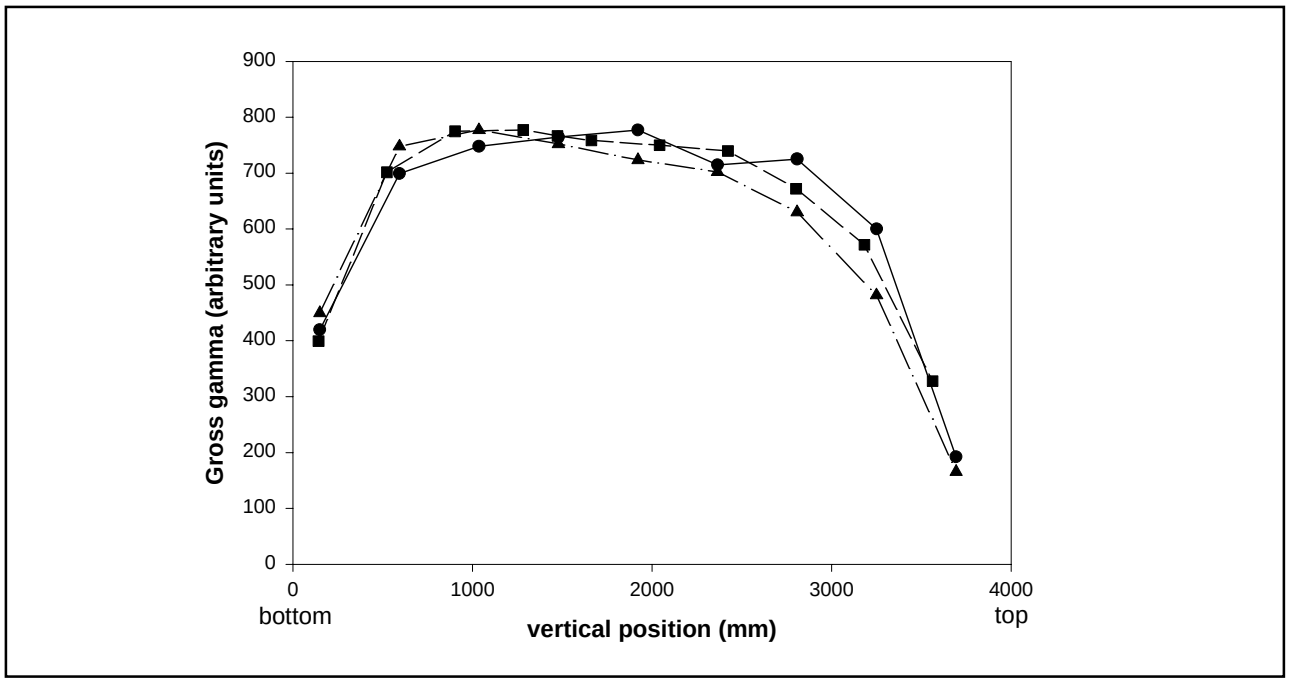

Figure 33. *Comparison of the gross gamma profiles of assemblies #6124, #12323 and #7055. Circles and solid line represent the assembly #6124, squares and dashed line the assembly #12323 and triangles and dash-dot line the assembly #7055, respectively.*

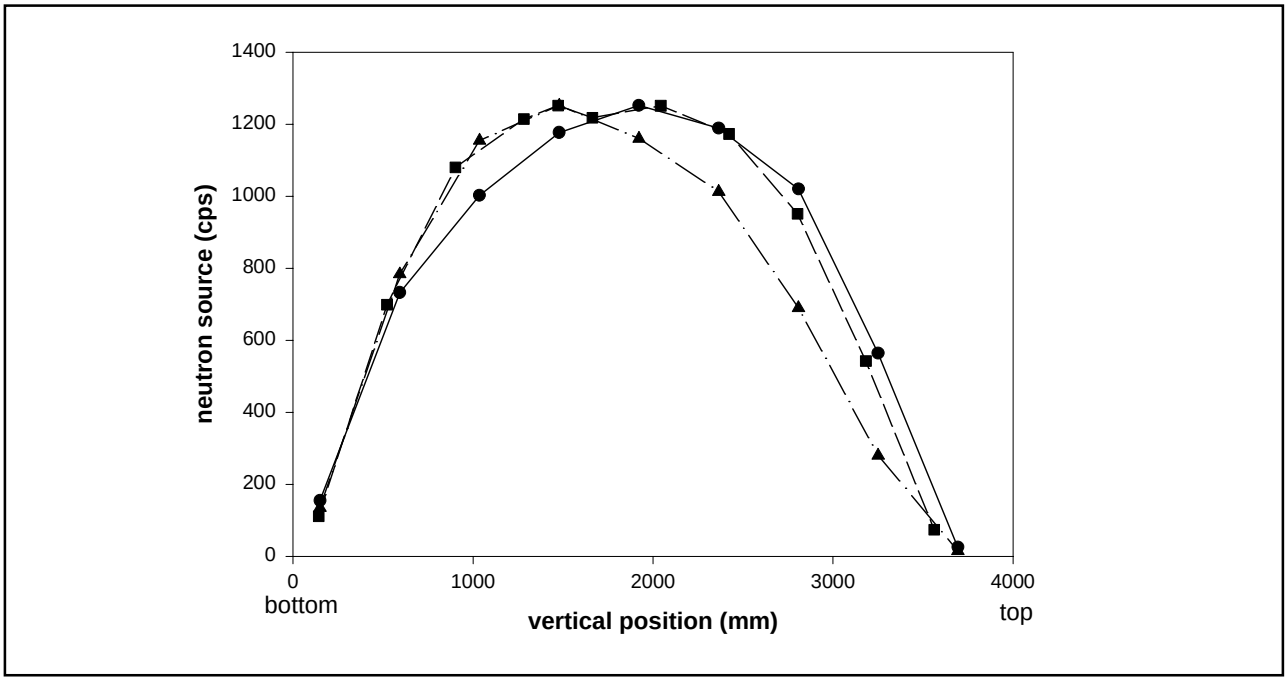

Figure 34. *Comparison of neutron profiles of assemblies #6124, #12323 and #7055. Circles and solid line represent the assembly #6124, squares and dashed line the assembly #12323 and triangles and dash-dot line the assembly #7055, respectively.*

8 SENSITIVITY TO VERTICAL POSITIONING

According to Tanskanen's ORIGEN-S calculations the void fraction has a strong influence on build-up of ^{244}Cm in BWR. This implies that for the same burnup a higher void fraction gives a higher neutron source. [11] Because of boiling the void fraction is larger in the upper part than in the lower part of an assembly. Owing to that, in December measurements were performed in addition to the mid-point (z=5705) at two additional heights 6275 and 5135, 570 mm above and below the mid-point.

All measured data points have been taken into consideration in the following fits. The measured raw data are shown in Table A1.IV in Annex 1.

The measurement data from all four sides were averaged and the corrections to the measurement data, as mentioned in section 6, have been made for A_{37}, gross gamma and neutron data. The analysis was made using the neutron counts from bare fission chambers, because the correlation between Cd-wrapped and bare neutron channels was perfectly linear.

The operator-declared burnup represents the average burnup of an assembly. On the other hand, both the measured gross gamma data and the spectroscopically obtained ^{137}Cs intensity reflect the burnup at the measurement height. Therefore one could expect that the variations in the axial burnup profiles, which are clearly seen in section 7, would influence on the measurement results.

In Figure 35 the ^{244}Cm neutron intensity is correlated to the gross gamma signal at three measurement heights according to equation (17). It seems that higher measurement level and higher void fraction implies higher ^{244}Cm neutron

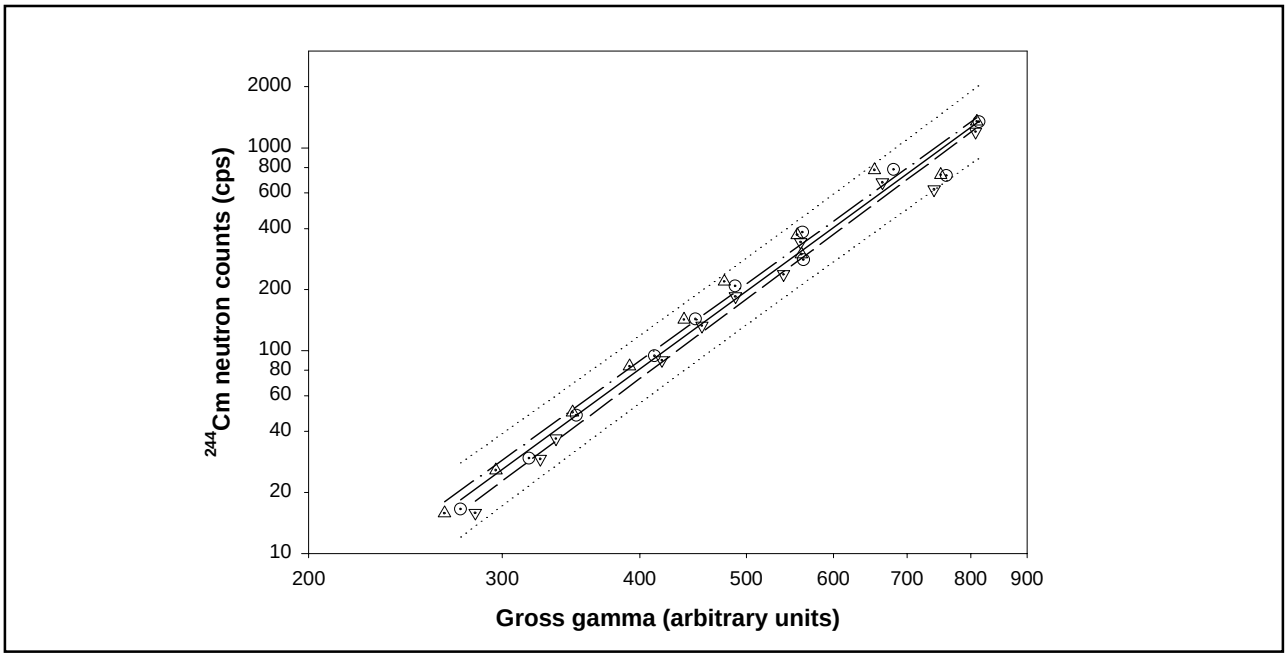

Figure 35. *^{244}Cm neutron counts vs. gross gamma signal at three heights. Triangles up and dash-dot regression line correspond to height 570 mm above the mid-point. Circles and solid regression line correspond to the mid-point. Triangles down and dashed regression line correspond to height 570 mm below the mid-point. Dotted lines represent the error corridor corresponding to the regression line at the mid-point.*

source. At high burnups this effect decreases due to different slopes of these three correlation curves. The parameters of the ^{244}Cm neutron counts vs. gross gamma fit are shown in Table XVII. At each height the ^{137}Cs peak intensity and the gross gamma have been correlated to the burnup according to equations (2) and (10). In addition, the ^{244}Cm neutron counts have been correlated to the burnup and ^{137}Cs peak intensity according to equations (15) and (16). The parameters received from these fittings are shown in Tables XIII–XVI.

The error corridor of the correlation curve at the mid-point is presented in Figure 35. All data points of all three heights are inside this error corridor. This implies that burnup profile variation and positioning in axial direction are not a considerable error source at least inside about one metre interval in the central part of an assembly. As a corollary, one calibration curve, ^{244}Cm neutrons versus gross gamma, should be quite generally valid for a certain type of fuel assemblies.

Table XIII. *Parameters of the ^{137}Cs peak intensity vs. burnup fit. LOW refers to height 570 mm below the mid-point, MID to the mid-point and HIGH to 570 mm above the mid-point.*

	k cps/MWdkg^{-1}	σ_k	σ_k/k	R^2
LOW	7.25	0.17	0.023	0.949
MID	7.31	0.19	0.026	0.939
HIGH	7.11	0.20	0.028	0.930
PYVO	7.31	0.02	0.003	0.999

Table XIV. *Parameters of the gross gamma vs. burnup fit.*

	k''	$\sigma_{k''}$	$\sigma_{k''}/k''$	R^2
LOW	19.71	0.31	0.016	0.973
MID	19.95	0.34	0.017	0.971
HIGH	19.56	0.37	0.019	0.965
PYVO	19.94	0.06	0.003	0.999

Table XV. *Parameters of the ^{244}Cm neutron counts vs. burnup fit.*

	a	σ_α	b	σ_b	R^2
LOW	–3.90	0.22	4.36	0.15	0.989
MID	–3.97	0.17	4.45	0.12	0.994
HIGH	–4.10	0.17	4.54	0.12	0.993
PYVO	–4.28	0.05	4.66	0.04	0.999

Table XVI. *Parameters of the ^{244}Cm neutron counts vs. ^{137}Cs peak intensity fit.*

	a'	$\sigma_{\alpha'}$	b'	$\sigma_{b'}$	R^2
LOW	–5.99	0.46	3.65	0.20	0.973
MID	–5.81	0.50	3.59	0.22	0.967
HIGH	–5.94	0.53	3.66	0.24	0.964
PYVO	–8.33	0.17	4.67	0.07	0.998

Table XVII. *Parameters of the ^{244}Cm neutron counts vs. gross gamma fit.*

	a''	$\sigma_{\alpha''}$	b''	$\sigma_{b''}$	R^2
LOW	–8.64	0.40	4.04	0.15	0.988
MID	–8.39	0.40	3.96	0.15	0.987
HIGH	–8.23	0.42	3.91	0.16	0.986
PYVO	–10.37	0.20	4.67	0.07	0.998

9 CONCLUSION

In the measurements performed in September and December 1999 using the upgraded fork detector, the calculated correlations of the measurement results are improved as compared to the corresponding correlations of the data measured in November 1998. Several reasons can be attributed to this improvement. First the data quality is improved, because

- the upgraded fork measures all signals on the same vertical level;
- the data on one vertical level was taken on all four sides of the assembly and these results were averaged;
- neutron data measured in November 1998 have been corrected only for cooling time whereas for the 1999 data both the ^{244}Cm share and the initial enrichment correction were applied.

As the measure of the burnup, three different signals were tested:

- spectrometrically measured ^{137}Cs peak intensity,
- raw gross gamma signal from a pair of ionisation chambers and
- gross gamma signal with subtraction of the contribution of ^{134}Cs and ^{106}Ru/Rh based on the spectrometric data.

The measurement results were reduced to the fuel discharge date and compared with the calculated values obtained by the PYVO code.

The ^{134}Cs and ^{106}Ru/Rh corrections on the gross gamma seem to be successful. The reason to this is probably that the gross gamma data are less sensitive to the positioning error than the measured ^{137}Cs activity data. The gross gamma signal with these corrections applied seems to be a good candidate for the measure of the burnup in neutron-to-burnup correlation. One calibration curve can be used for three different BWR assembly types of similar design. These hypotheses need additional experimental verification, before they can be generally adopted. Separate burnup verification can be performed using the gross gamma vs. burnup reference curve.

When the spent fuel assemblies are disposed of into the final repository they will obviously have such long cooling times that the gamma spectrometric corrections in gross gamma signal would not be needed. The gross gamma signal would consist predominantly of the gamma emission of ^{137}Cs while other isotopes have decayed off. However, the gamma spectroscopic measurements are important to verify that the gross gamma signal does not include abnormal isotopes originating e.g. from irradiated dummy rods.

The measurement time was 100 s in these measurements. It is adequate for making the gamma spectrometric corrections to the gross gamma signal. If the Cs-ratio (^{134}Cs/^{137}Cs) were used as a measure of burnup, a considerably longer measurement time would be required. It would increase the costs and reduce the smoothness of the measurements. In addition, it is not an option when the spent fuel assemblies with long cooling time are disposed of into the final repository, because the ^{134}Cs has already decayed off. Also in these measurements many assemblies were so old that the Cs -ratio could not be used as a measure of burnup.

In the analysis of the data the correction for the share of ^{244}Cm neutrons in the measured neutron count rate was taken into account based on the results obtained from calculations with PYVO. In addition, the calculated ^{244}Cm neutron source and the ^{137}Cs activity of the measured assemblies were obtained with help of the PYVO code. All in all, PYVO can be considered as an essential tool in the analysis of neutron and gamma data for partial defect verification purpose.

Because the measured assemblies have differ-

ent initial enrichments, the measured neutron data have been corrected to a certain reference enrichment value. The enrichment correction based on the calculations made with ORIGEN-S seems to be worthwhile. Enrichment corrected ^{244}Cm neutrons correlate much better to the burnup and gross gamma than the neutron data without the enrichment correction.

Using the operator declared data is inevitable in order to calculate the necessary corrections to the measured neutron and gamma data. The evacuation date from reactor is needed for cooling time correction of the measured data. The burnup and initial enrichment values of the assemblies are essential data for the enrichment correction on the neutron signal and to calculate the ^{244}Cm share of the total neutron counts. Cooling time, irradiation days and possible off-reactor cycles of the assemblies are needed in calculation of the ^{244}Cm share of the total neutron counts.

The multiplication of the ^{244}Cm neutrons has not been taken into consideration in the analysis of the measurement data. The multiplication factor depends on the burnup and the initial enrichment of the assemblies. The value of the multiplication factor increases as the burnup decreases or as the initial enrichment increases. [17] The analysis method could be developed further by investigating the need and possibility to correct the measured neutron data for the multiplication of the neutrons.

There are two options, which may have potential as a reference curve for partial defect purposes. One is that the ^{244}Cm neutron counts are correlated to the gross gamma data. The other is that the ^{244}Cm neutron counts are correlated to the declared burnup and the burnup data are verified separately. ^{244}Cm neutron counts correlate better to operator declared burnup data than to the measured gross gamma data.

REFERENCES

1 P. M. Rinard and G. E. Bosler. Safeguarding LWR Spent Fuel with the Fork Detector. LA-11096-MS. Los Alamos, NM, 1988. 82 pp.

2 R. Arlt. Technical Report on First Test of a New Underwater Gamma Spectrometer (UWGS) Used in Conjunction with the fork Detector. December 1, 1998.

3 P.A. Aarnio, M. T. Nikkinen and J. T. Routti. SAMPO, Advanced Gamma Spectrum Analysis Software, Version 4.00. User's Guide, Espoo, 1999.

4 R. Gunnink, A Guide for Using CsRatio, PC Version 1.1 for DOS and Windows. December 1998.

5 SigmaPlot 5.0 Programming Guide, SPSS Inc., Chicago, Ill., U.S.A., 1998.

6 SCALE Manual – Version 4.4 (Draft).

7 M. Samson, J.P. Grouillet, J. Pavageau, P. Marimbeau, J. Pinel, J.M. Vidal. CESAR: A Simplified Evolution Code for Reprocessing Applications. ENC'98. Nice (25–28 October).

8 Bignan, M. Boschiero, F. Poncelet, L. Martin-Deidier, J. Romeyer-Dherbey. Active and passive non-destructive measurements for fuel assemblies nuclear monitoring. Third International Conference on Nuclear Fuel Reprocessing and Waste Management. RECOD'91 Sendai Japan (1991).

9 R. Berne, G. Bignan, G. Andrieu, D. Dethan. A versatile passive and active non-destructive device for spent fuel assemblies monitoring. International Conference on Nuclear Waste Management and Environmental Remediation. Prague (September 1993).

10 G. Bignan, D. Janvier. NAJA. A new non-destructive automatic on line device for fuel assembly characterization and core load conformity control. ANS meeting "Advances in Nuclear Fuel Management II". Myrtle Beach (March 1997).

11 Tanskanen. Assessment of the neutron and gamma sources of the spent BWR fuel. Interim report on Task FIN JNT A 1071 of the Finnish Support Programme to IAEA safeguards. STUK-YTO-TR 170. Helsinki 2000. 17 pp + Appendices 14 pp.

12 Tarvainen, A. Bäcklin, A. Håkansson. Calibration of the TVO spent BWR reference fuel assembly. Final report on the joint Task JNT61 of the Finnish and Swedish Support Programmes to IAEA Safeguards. STUK-YTO-TR 37. Helsinki 1992. 49 pp.

13 Tarvainen, F. Lévai, T. Valentine, M. Abhold, B. Moran. NDA techniques for spent fuel verification and radiation monitoring. Report on Activities 6a and 6b of Task JNT C799 (SAGOR). Finnish Support Programme to the IAEA Safeguards. STUK-YTO-TR 133. Helsinki 1997. 23 pp. + Annexes 24 pp.

14 R.B. Firestone, S.Y Frank Chu (CD-ROM editor), C.M Baglin (editor). Table of Isotopes. Eighth Edition. 1998 Update with CD-ROM. Lawrence Berkley National Laboratory, University of California.

15 H. Würz. A simple nondestructive measurement system for spent-fuel management. Nuclear Technology, Vol. 95, 1991, pp. 193–206.

16 M. Anttila. Gamma and neutron dose rates on the outer surface of the nuclear waste disposal canisters. Posiva report 96-10, 1996.

17 H. Menlove, Private communication, June 2000.

ANNEX 1 MEASURED RAW DATA

Table A1.I. *Raw data of the gamma spectrometric scanning of the assembly #12350 (y = 5705 mm). "Non-corr" denotes the values which are not corrected for the cooling time.*

Angle (degrees)	Spectrum Filename	non-corr A_{37} (cps)	non-corr $A_{34,605}$ (cps)	non-corr $A_{34,795}$ (cps)	non-corr A_{34}/A_{37}
0	f12350_1	290	47.2	31.9	0.1322
5	f12350_2	336.8	53.5	35.7	0.1286
10	f12350_3	328.4	51.4	34.7	0.1271
15	f12350_4	320.4	50.8	31.2	0.1259
20	f12350_5	315.8	53.2	33.9	0.1349
5	f12350_6	343.7	54.5	35.1	0.1273
0	f12350_7	315.5	54.4	32.4	0.1360
-5	f12350_8	294.8	45	29.6	0.1232
-10	f12350_9	290.7	47.9	32.5	0.1340
-15	f12350_a	308	44.6	31	0.1185
-20	f12350_b	305.5	50.2	30.8	0.1305
-35	f12350_c	308.8	49.3	35.5	0.1318
-45	f12350_d	306.3	46.2	31.8	0.1231
-40	f12350_e	308.1	49.8	32.1	0.1298
-35	f12350_f	310.6	48.5	31	0.1252
-30	f12350_g	317.1	44.9	32.6	0.1171
-25	f12350_h	311.2	46.2	33.2	0.1225
-20	f12350_l	309.4	50.3	31.5	0.1297
-15	f12350_j	312.7	49.4	32.7	0.1277
-10	f12350_k	293.2	42.2	29.4	0.1178
-5	f12350_l	285.4	43.6	28.2	0.1228
0	f12350_m	317.1	48.3	34.5	0.1255
5	f12350_n	332.1	53.8	35.2	0.1306
10	f12350_o	326.8	46.9	34.5	0.1191
15	f12350_p	324.8	51.5	31.1	0.1254
20	f12350_q	314.6	44.4	30.7	0.1153
25	f12350_r	315.4	47.7	33.8	0.1243
30	f12350_s	307.3	48.7	30.3	0.1262
35	f12350_t	311.3	47.6	32.3	0.1243
40	f12350_u	302.8	48.7	30.1	0.1279
45	f12350_v	299.8	45	31.8	0.1233
50	f12350_w	292.8	45.7	31.7	0.1276

Table A1.II. *Raw data of the measurement when the assembly #12350 was moved towards the measurement head (z = 5705 mm).*

x-coordinate (cm)	Spectrum Filename	non-corr A_{37} (cps)	non-corr $A_{34,605}$ (cps)	non-corr $A_{34,795}$ (cps)	non-corr A_{34}/A_{37}
0	a12350_5	211.1	29.8	22.5	0.1180
-1	a12350_6	231.6	34.9	23	0.1217
-2	a12350_7	264.1	36.8	26.3	0.1148
-3	a12350_8	303.5	47.3	31.2	0.1259
-4	a12350_9	338.3	53.3	34.9	0.1270

MEASURED RAW DATA **ANNEX 1**

Table A1.III. *Raw data of the measurements performed at the position z = 5705 mm and x = 0 mm in September campaign.*

Ass. ID	Angle (degrees)	Spectrum Filename	non-corr N(Cd) (cps)	non-corr N(noCd) (cps)	non-corr G (arbitrary units)	non-corr A_{37} (cps)	non-corr $A_{34,605}$ (cps)	non-corr $A_{34,795}$ (cps)	non-corr A_{34}/A_{37}
10003	**0**	**a10003_1**	**110.71**	**187.01**	**479.4**	**131.4**	**6**	**3.4**	**0.0356**
	90	a10003_2	115.82	192.45	479.4	135.4			0
	270	a10003_3	113.12	189.01	486.9	147.3			0
	180	a10003_4	115.44	190.97	480	150.5			0
9367	**0**	**a9367_1**	**150.02**	**250.29**	**518.8**	**147.6**			**0**
	90	a9367_2	152.06	255.57	507.5	159.9			0
	270	a9367_3	147.97	247.34	501.9	146.6	4.8	3.2	0.0265
	180	a9367_4	153.84	255.7	505.6	155.5	7.6	4.6	0.0387
12338	**0**	**a12338_1**	**295.85**	**505.51**	**691.9**	**185.2**	**20.4**	**13.1**	**0.0884**
	90	a12338_2	300.95	515.01	696.3	189.1	20.7	14.6	0.0899
	270	a12338_3	303.08	518.35	693.8	194.3	19.6	14.7	0.0842
	180	a12338_4	298.26	506.41	713.8	195.5	20.3	13.9	0.0846
6124	**0**	**a6124_e**	**400.6**	**694.8**	**568.1**	**183.8**	**5.9**	**2.6**	**0.0238**
	90	a6124_f	401.41	697.12	555.6	182			0
	270	a6124_g	396.73	688.72	560.6	190.4	4.6	3.3	0.0199
	180	a6124_h	404.79	703.76	550.6	176.9			0
13857	**0**	**a13857_1**	**228.59**	**384.47**	**735**	**192.9**	**21.6**	**14.3**	**0.0905**
	90	a13857_2	227.11	382.99	721.9	191.9	22.4	14.4	0.0937
	270	a13857_3	229	386.88	733.1	194.9	22.8	17.1	0.0976
	180	a13857_4	226.36	384.25	731.9	192.7	25.3	15.9	0.1048
0104	**0**	**a0104_1**	**188.29**	**318.16**	**572.5**	**168.2**	**12**	**7.8**	**0.0574**
	90	a0104_2	196.83	329.23	569.4	169.8	14.5	9.3	0.0685
	270	a0104_3	190.08	320.44	568.8	162.9	11	8.3	0.0564
	180	a0104_4	193.81	327.26	576.9	177.2	13.3	9.3	0.0615
12350	**0**	**a12350_a**	**387.65**	**675.44**	**805.6**	**220.3**	**36**	**21.8**	**0.1293**
	90	a12350_b	388.61	680.58	818.1	241.3	36.5	25.7	0.1242
	270	a12350_c	388.14	672.97	805	213.8	33.3	24	0.1286
	180	a12350_d	395.65	681.84	800.6	221.3	32	23.4	0.1198
10181	**0**	**a10181_1**	**266.3**	**466.12**	**688.1**	**190.6**	**20**	**13.8**	**0.0857**
	90	a10181_2	271.77	470.86	681.9	187.4	19.1	13.2	0.0833
	270	a10181_3	268.33	463.2	686.3	191.1	19.1	12.7	0.0809
	180	a10181_4	272.93	468.34	678.8	177.5	18.8	11.9	0.0847
12387	**0**	**a12387_1**	**151.14**	**255.77**	**529.4**	**147.8**			**0**
	90	a12387_2	157.8	264.1	524.4	155.2	7.2	6.3	0.0404
	270	a12387_3	152.59	255.4	517.5	144.1	8.8	5	0.0477
	180	a12387_4	157.53	263.49	516.9	150.1	8.7	5.6	0.0465
12500	**0**	**a12500_1**	**145.8**	**243.55**	**523.8**	**157.3**	**7.4**	**5.3**	**0.0388**
	90	a12500_2	146.84	246.37	518.1	153.9	8.8	5.1	0.0448
	270	a12500_3	143.85	238.69	513.8	148.5			0
	180	a12500_4	149.67	247.13	511.9	154.8	8.4	5.7	0.0441
7472	**0**	**a7472_1**	**76.53**	**123.93**	**381.9**	**118.3**			**0**
	90	a7472_2	75.56	123.09	383.1	117.8			0
	270	a7472_3	75.12	120.96	374.4	112.2			0
	180	a7472_4	77.02	124.23	376.3	111.6			0
7516	**0**	**a7516_1**	**101.06**	**165.04**	**403.1**	**136.4**			**0**
	90	a7516_2	100.94	166.77	401.9	140.1			0
	270	a7516_3	99.18	162.92	405	123.2			0
	180	a7516_4	101.9	167.38	405.6	129.7			0

ANNEX 1 MEASURED RAW DATA

Table A1.III. *continues.*

Ass. ID	Angle (degrees)	Spectrum Filename	non-corr N(Cd) (cps)	non-corr N(noCd) (cps)	non-corr G (arbitrary units)	non-corr A_{37} (cps)	non-corr $A_{34,605}$ (cps)	non-corr $A_{34,795}$ (cps)	non-corr A_{34}/A_{37}
7055	**0**	**a7055_a**	**39.36**	**62.9**	**248**	**75.2**			**0**
	90	a7055_b	41.12	65.85	245.8	78			0
	270	a7055_c	39.94	64.36	248	74.9			0
	180	a7055_d	40.37	64.99	252.5	79.7			0
12366	**0**	**a12366_1**	**189.46**	**318.82**	**555.6**	**167**	**10.3**	**7.9**	**0.0518**
	90	a12366_2	192.04	320.04	550	162.8	10.1	7.5	0.0516
	270	a12366_3	190.5	316.79	546.9	154.4	10.5	6.4	0.0539
	180	a12366_4	192.32	321.37	549.4	164.2	9.9	6.2	0.0481
10475	**0**	**a10475_1**	**108.57**	**179.12**	**464.4**	**143.1**			**0**
	90	a10475_2	109.02	180.25	456.9	141.4			0
	270	a10475_3	109.73	179.75	462.5	151.6	6.1	3.3	0.0311
	180	a10475_4	107.32	176.1	458.8	146.9			0
12323	**0**	**a12323_1**	**306.89**	**520.54**	**694.4**	**191.5**	**22.7**	**16.3**	**0.0978**
	90	a12323_2	311.09	529.63	703.8	202.6	21.3	15.6	0.0872
	270	a12323_3	294.26	513.92	687.5	184	20.5	14.3	0.0912
	180	a12323_4	303.22	526.7	700	191.4	23	14.1	0.0954
6124	**0**	**a6124_a**	**391.99**	**687**	**557.5**	**179.3**	**4.6**	**2.9**	**0.0205**
	90	a6124_b	399.61	697.81	553.1	181.3			0
	270	a6124_c	391.13	683.87	548.1	167.8			0
	180	a6124_d	399,37	699,24	556,3	186			0

MEASURED RAW DATA **ANNEX 1**

Table A1.IV. *Raw data of the measurements performed at three different heights z = 5135 mm, z = 5705 mm and z = 6275 mm when x = 0 mm in December campaign.*

Ass. ID	Height (mm)	Angle (deg)	non-corr N_{Cd} (cps)	Error N_{Cd} (cps)	non-corr $N_{no\text{-}Cd}$ (cps)	Error $N_{no\text{-}Cd}$ (cps)	non-corr G	Error G	non-corr A_{37} (cps)	Error A_{37} (%)	non-corr $A_{34,605}$ (cps)	Error $A_{34,605}$ (%)	non-corr $A_{34,795}$ (cps)	Error $A_{34,795}$ (%)	non-corr A_{34}/A_{37}
12323	**5135**	**0**	**304.27**	**1.74**	**484.32**	**2.20**	**642.5**	**0.313**	**200.9**	**0.9**	**17**	**6.3**	**13.8**	**4.3**	**0.0722**
		90	314.03	1.77	490.40	2.21	651.3	0.313	208.7	0.9	22.6	5	14.2	4.5	0.0864
		270	301.04	1.74	481.57	2.19	645.0	0.313	200.4	0.9	18.2	5.8	12.2	4.9	0.0736
		180	306.67	1.75	488.88	2.21	638.1	0.313	190.3	0.9	19.6	5.5	13	4.6	0.0833
	5705	0	352.90	1.88	561.52	2.37	651.9	0.313	190	1	19.4	5.7	13.6	4.4	0.0837
		180	363.23	1.91	568.90	2.39	666.3	0.313	202.8	0.9	19.6	5.4	13.6	4.6	0.0790
		270	353.03	1.88	556.14	2.36	658.8	0.313	192.2	1	19.3	5.5	12.8	4.8	0.0812
		90	365.42	1.91	567.58	2.38	674.4	0.313	211.2	0.9	20.7	5.5	14.9	4.3	0.0809
	6275	0	346.82	1.86	561.16	2.37	636.9	0.313	186.6	1	18.8	5.5	13.6	4.5	0.0833
		90	362.53	1.90	565.76	2.38	658.1	0.313	200.8	0.9	22.3	4.9	14.5	4.3	0.0894
		270	335.75	1.83	545.16	2.33	622.5	0.313	163.3	1	17	5.8	12.8	4.5	0.0869
		180	366.03	1.91	569.28	2.39	663.8	0.313	192.6	1	21.5	5	14	4.6	0.0899
4468	**5135**	**0**	**15.99**	**0.40**	**27.40**	**0.52**	**187.2**	**0.0775**	**61**	**1.4**					**0**
		90	17.15	0.41	27.23	0.52	190.9	0.202	62.7	1.4					0
		270	16.84	0.41	28.79	0.54	190.3	0.0775	67.7	1.4					0
		180	17.32	0.42	28.26	0.53	188.1	0.0775	64.8	1.4					0
	5705	180	18.31	0.43	30.79	0.55	187.8	0.286	64.6	1.4					0
		270	18.07	0.43	30.11	0.55	182.7	0.202	60.2	1.5					0
		0	17.55	0.42	26.96	0.52	181.8	0.143	62.9	1.4					0
		90	17.05	0.41	28.69	0.54	181.4	0.0775	56.7	1.5					0
	6275	90	16.83	0.41	27.22	0.52	175.2	0.0775	56.7	1.5					0
		0	17.20	0.41	26.43	0.51	177.3	0.0775	58.4	1.5					0
		270	17.93	0.42	29.12	0.54	181.1	0.143	69.7	1.4					0
		180	17.73	0.42	28.54	0.53	175.7	0.0775	58.6	1.5					0
4469	**5135**	**0**	**29.64**	**0.54**	**45.84**	**0.68**	**218.2**	**0.0775**	**78.9**	**1.3**					**0**
		90	27.23	0.52	45.76	0.68	214.5	0.143	67.6	1.4					0
		270	30.35	0.55	48.34	0.70	218.5	0.0775	80.9	1.3					0
		180	29.15	0.54	46.48	0.68	216.0	0.0775	71.5	1.4					0
	5705	180	28.95	0.54	47.01	0.69	210.4	0.286	71.6	1.3					0
		270	29.79	0.55	47.00	0.69	212.0	0.0775	78.7	1.3					0
		0	29.68	0.54	46.54	0.68	213.7	0.0775	77.7	1.3					0
		90	28.51	0.53	47.32	0.69	210.8	0.0775	72.7	1.3					0
	6275	90	25.19	0.50	41.23	0.64	199.6	0.0775	69.8	1.4					0
		0	25.19	0.50	40.30	0.63	193.5	0.143	69.8	1.4					0
		270	25.34	0.50	41.82	0.65	197.4	0.0775	69.5	1.4					0
		180	25.68	0.51	40.73	0.64	199.6	0.0775	73	1.3					0
7121	**5135**	**0**	**35.43**	**0.60**	**57.04**	**0.76**	**236.5**	**0.0775**	**83.4**	**1.3**					**0**
		90	33.82	0.58	56.24	0.75	230.3	0.247	74.2	1.3					0
		270	37.34	0.61	58.48	0.76	239.1	0.0775	85.7	1.3					0
		180	33.95	0.58	56.15	0.75	231.8	0.247	77.9	1.3					0
	5705	0	45.85	0.68	74.96	0.87	244.9	0.0775	86.3	1.3					0
		90	44.53	0.67	73.65	0.86	242.2	0.0775	80.1	1.3					0
		270	47.08	0.69	74.19	0.86	245.8	0.286	84.5	1.3					0
		180	44.58	0.67	74.00	0.86	245.6	0.0775	87.2	1.2					0
	6275	0	46.49	0.68	76.36	0.87	240.4	0.202	81.1	1.3					0
		90	46.77	0.68	75.75	0.87	242.7	0.0775	83.5	1.3					0
		270	47.52	0.69	78.60	0.89	240.8	0.0775	81.2	1.3					0
		180	48.65	0.70	76.12	0.87	246.9	0.0775	91.3	1.2					0

ANNEX 1 MEASURED RAW DATA

Table A1.IV. *continues.*

Ass. ID	Height (mm)	Angle (deg)	non-corr N_{Cd} (cps)	Error N_{Cd} (cps)	non-corr $N_{no\text{-}Cd}$ (cps)	Error $N_{no\text{-}Cd}$ (cps)	non-corr G	Error G	non-corr A_{37} (cps)	Error A_{37} (%)	non-corr $A_{34,605}$ (cps)	Error $A_{34,605}$ (%)	non-corr $A_{34,795}$ (cps)	Error $A_{34,795}$ (%)	non-corr A_{34}/A_{37}
7289	**5135**	**0**	**82.69**	**0.91**	**133.84**	**1.16**	**304.4**	**0.0775**	**115.4**	**1.1**					**0**
		90	81.68	0.90	131.19	1.15	291.1	0.286	96.2	1.2					0
		270	85.77	0.93	136.50	1.17	308.8	0.202	124.4	1.1					0
		180	82.57	0.91	135.25	1.16	293.6	0.0775	101.5	1.2					0
	5705	0	88.85	0.94	141.30	1.19	297.7	0.0775	107.1	1.1					0
		90	86.12	0.93	139.87	1.18	288.4	0.0775	95.3	1.2					0
		270	91.63	0.96	141.28	1.19	301.6	0.202	121.9	1.1					0
		180	87.07	0.93	140.73	1.19	291.7	0.0775	100.4	1.2					0
	6275	0	78.33	0.89	124.75	1.12	279.5	0.0775	96.3	1.2					0
		90	77.23	0.88	125.30	1.12	275.0	0.0775	93	1.2					0
		270	81.74	0.90	125.76	1.12	285.0	0.143	113.7	1.1					0
		180	79.17	0.89	125.16	1.12	279.6	0.0775	101.3	1.2					0
7543	**5135**	**0**	**57.12**	**0.76**	**95.08**	**0.98**	**327.5**	**0.313**	**113.4**	**1.1**					**0**
		90	61.67	0.79	96.78	0.98	325.0	0.313	115.2	1.1					0
		270	60.18	0.78	92.97	0.96	326.9	0.313	114.4	1.1					0
		180	59.82	0.77	94.93	0.97	325.6	0.313	112.8	1.1					0
	5705	0	61.72	0.79	100.33	1.00	319.4	0.313	108	1.1					0
		90	64.34	0.80	103.73	1.02	323.7	0.313	112.9	1.1					0
		270	61.79	0.79	100.26	1.00	320.6	0.313	109.3	1.1					0
		180	65.12	0.81	104.57	1.02	323.7	0.313	113.9	1.1					0
	6275	0	61.80	0.79	101.56	1.01	307.7	0.143	102	1.2					0
		90	66.07	0.81	103.96	1.02	319.4	0.313	116.8	1.1					0
		270	62.79	0.79	98.59	0.99	309.1	0.286	104.4	1.2					0
		180	68.71	0.83	102.87	1.01	320.6	0.313	117.7	1.1					0
6110	**5135**	**0**	**81.82**	**0.90**	**127.16**	**1.13**	**345.6**	**0.313**	**147.3**	**1**					**0**
		90	77.65	0.88	125.55	1.12	318.7	0.313	109.1	1.1					0
		270	82.66	0.91	126.42	1.12	345.6	0.313	146.3	1					0
		180	78.05	0.88	127.88	1.13	325.0	0.313	109	1.1					0
	5705	0	92.94	0.96	141.77	1.19	343.7	0.313	141.6	1					0
		90	87.87	0.94	144.66	1.20	320.6	0.313	108.9	1.1					0
		270	92.40	0.96	142.19	1.19	343.1	0.313	144.3	1					0
		180	89.87	0.95	142.11	1.19	326.9	0.313	111.9	1.1					0
	6275	0	99.42	1.00	149.44	1.22	338.8	0.313	135.3	1					0
		90	95.98	0.98	152.28	1.23	322.5	0.313	112.5	1.1					0
		270	97.95	0.99	149.68	1.22	338.8	0.313	135.6	1					0
		180	92.47	0.96	149.31	1.22	304.3	0.0775	95.3	1.2					0
10048	**5135**	**0**	**107.46**	**1.04**	**168.02**	**1.30**	**440.6**	**0.313**	**176.1**	**0.9**	**5.7**	**13**	**4**	**9**	**0.0265**
		90	106.49	1.03	169.18	1.30	434.4	0.313	158.7	1					0
		270	109.95	1.05	165.20	1.29	439.4	0.313	164.7	1	7.1	10.5	4	9	0.0336
		180	112.43	1.06	165.01	1.28	439.4	0.313	183.5	0.9	6.9	11.4	4.9	7.9	0.0309
	5705	0	127.96	1.13	200.52	1.42	455.0	0.313	178.9	0.9					0
		90	127.56	1.13	199.94	1.41	451.3	0.313	172	1	6.9	11.5	4.5	8.2	0.0323
		270	130.60	1.14	193.77	1.39	453.8	0.313	171.6	1	2.6	31.3	4.1	8.6	0.0164
		180	129.00	1.14	193.77	1.39	456.3	0.313	193.5	0.9	7.6	11.2	4.7	8.9	0.0312
	6275	0	136.35	1.17	212.29	1.46	454.4	0.313	169.5	1	6.4	11.6	3.7	9.5	0.0296
		90	138.75	1.18	211.83	1.46	455.0	0.313	179.3	0.9	6.7	11.9	4.7	8.7	0.0306
		270	140.58	1.19	208.86	1.45	453.1	0.313	162.6	1					0
		180	141.34	1.19	206.94	1.44	458.1	0.313	197.2	0.9	7.4	11.2	5.3	7.5	0.0309

MEASURED RAW DATA **ANNEX 1**

Table A1.IV. *continues.*

Ass. ID	Height (mm)	Angle (deg)	non-corr N_{Cd} (cps)	Error N_{Cd} (cps)	non-corr $N_{no\text{-}Cd}$ (cps)	Error $N_{no\text{-}Cd}$ (cps)	non-corr G	Error G	non-corr A_{37} (cps)	Error A_{37} (%)	non-corr $A_{34,605}$ (cps)	Error $A_{34,605}$ (%)	non-corr $A_{34,795}$ (cps)	Error $A_{34,795}$ (%)	non-corr A_{34}/A_{37}
13285	**5135**	**0**	**168.66**	**1.30**	**264.40**	**1.63**	**650.0**	**0.313**	**181.6**	**1**	**25.7**	**4.5**	**17.7**	**3.7**	**0.1155**
		90	158.51	1.26	259.09	1.61	604.4	0.313	138.1	1.1	22.4	4.4	14.7	3.9	0.1308
		270	164.95	1.28	262.71	1.62	640.0	0.313	171.1	1	27.1	4.1	18	3.8	0.1281
		180	173.59	1.32	268.69	1.64	666.9	0.313	191.4	1	30.3	4	20.7	3.4	0.1289
	5705	0	185.81	1.36	295.79	1.72	660.6	0.313	174.2	1	28.1	4	20.3	3.5	0.1333
		90	179.16	1.34	291.33	1.71	628.1	0.313	148.1	1.1	24.5	4.4	16.2	4	0.1337
		270	183.76	1.36	294.37	1.72	650.0	0.313	162	1	26	4.2	19.1	3.7	0.1332
		180	192.01	1.39	298.08	1.73	685.0	0.313	207.8	0.9	37.1	3.4	24.9	3.3	0.1448
	6275	0	180.11	1.34	284.54	1.69	641.3	0.313	161.6	1	25.1	4.4	18.1	3.7	0.1283
		90	178.77	1.34	289.53	1.70	626.3	0.313	148.4	1.1	22.6	4.6	16.9	3.8	0.1270
		270	177.24	1.33	282.85	1.68	631.9	0.313	154.7	1.1	25	4.4	18	3.8	0.1334
		180	190.95	1.38	287.12	1.69	675.6	0.313	211.6	0.9	36	3.5	26.1	3	0.1407
16732	**5135**	**0**	**365.56**	**1.91**	**554.55**	**2.35**	**1362.0**	**1.25**	**283.3**	**1**	**107.7**	**2.3**	**76.4**	**2.1**	**0.3126**
		90	347.11	1.86	548.86	2.34	1272.0	1.25	211.4	1.1	89.3	2.5	61.8	2.3	0.3452
		270	368.35	1.92	547.76	2.34	1352.0	1.25	267	1	107.3	2.3	75.1	2.1	0.3293
		180	369.32	1.92	549.84	2.34	1360.0	1.25	252.8	1.1	103.9	2.2	77.4	2.1	0.3423
	5705	0	432.77	2.08	643.98	2.54	1453.0	1.25	273.8	1	112	2.2	81.1	2	0.3382
		90	416.70	2.04	647.05	2.54	1395.0	1.25	237.9	1.1	106.5	2.3	74.6	2.1	0.3669
		270	427.41	2.07	636.85	2.52	1423.0	1.25	256	1.1	113.6	2	74.1	2.2	0.3574
		180	432.67	2.08	649.92	2.55	1453.0	1.25	268	1.1	125.7	2	89.1	1.9	0.3856
	6275	0	440.50	2.10	650.20	2.55	1463.0	1.25	267.9	1	112.2	2.3	83.5	2	0.3487
		90	430.13	2.07	656.95	2.56	1430.0	1.25	254.5	1.1	119.2	2.1	80.1	2.1	0.3800
		270	423.50	2.06	643.05	2.54	1408.0	1.25	234.5	1.1	103.7	2.2	72.7	2.1	0.3626
		180	441.22	2.10	651.95	2.55	1463.0	1.25	268.8	1.1	130.6	2	86.4	2.1	0.3926
0425	**5135**	**0**	**533.32**	**2.31**	**829.65**	**2.88**	**1114.0**	**0.313**	**265**	**0.9**	**71.7**	**2.6**	**48.1**	**2.5**	**0.2194**
		90	520.76	2.28	830.56	2.88	1078.0	0.313	239.7	1	62.7	2.8	45	2.6	0.2157
		270	510.98	2.26	817.12	2.86	1083.0	0.313	237.8	1	64.7	2.7	42.7	2.7	0.2197
		180	531.64	2.31	835.10	2.89	1100.0	0.313	253.1	0.9	67.1	2.7	49	2.5	0.2196
	5705	0	596.01	2.44	924.06	3.04	1131.0	0.313	258.5	1	70.1	2.7	49.2	2.5	0.2224
		90	595.99	2.44	934.57	3.06	1116.0	0.313	251.9	1	72	2.5	48.6	2.4	0.2321
		270	578.75	2.41	915.06	3.02	1101.0	0.313	236.4	1	66.7	2.6	48.2	2.5	0.2331
		180	605.69	2.46	939.11	3.06	1140.0	0.313	265	0.9	75	2.5	52.6	2.4	0.2321
	6275	0	592.97	2.44	925.97	3.04	1116.0	0.313	239.6	1	67.4	2.8	44.7	2.5	0.2275
		90	611.34	2.47	947.59	3.08	1126.0	0.313	252.8	1	73.7	2.6	51	2.4	0.2382
		270	582.01	2.41	911.21	3.02	1097.0	0.313	223.5	1	63.3	2.7	42.6	2.7	0.2298
		180	633.28	2.52	939.69	3.07	1152.0	0.313	275.1	1	81.3	2.4	51.9	2.4	0.2368

ANNEX 1 MEASURED RAW DATA

Table A1.V. *Raw data of the axial scanning measurements of assemblies #7055 and #6124 (x=0 mm, angle =0 degrees).*

Assembly ID	Position	Spectrum Filename	non-corr N_{Cd} (cps)	non-corr $N_{no\text{-}Cd}$ (cps) (cps)	non-corr G (arbitrary units)	non-corr A_{37} (cps)	non-corr $A_{34,605}$ (cps)	non-corr $A_{34,795}$ (cps)	non-corr A_{34}/A_{37}
7055	**4382**	**a7055_1**	**4.44**	**6.88**	**148.3**	**48.2**			**0**
	4825	a7055_2	24.98	39.98	246.6	78.1			0
	5268	a7055_3	36.11	58.9	256.3	78.9			0
	5711	a7055_4	39.08	63.86	248	74.4			0
	6154	a7055_5	37.03	59.17	238.5	67			0
	6597	a7055_6	31.88	51.67	231.5	64.5			0
	7040	a7055_7	22.67	35.19	207.8	51.5			0
	7483	a7055_8	9.23	14.3	158.8	41.7			0
	7926	a7055_9	0.59	0.79	54.6	0			0
6124	**4382**	**a6124_1**	**54.67**	**89.93**	**316.9**	**108.3**	**2.8**	**0.9**	**0.0183**
	4825	a6124_2	246.33	424.87	503.8	159.2			0
	5268	a6124_3	336	581.46	538.8	170.3			0
	5711	a6124_4	389.62	682.64	550.6	172.5			0
	6154	a6124_5	413.66	726.24	560	178.9			0
	6597	a6124_6	395.62	689.91	547.5	169.8	5.3	2.9	0.0242
	7040	a6124_7	337.68	591.59	522.5	153.3			0
	7483	a6124_8	192.79	327.24	432.5	129			0
	7926	a6124_9	9.8	15.05	138.2	0			0

Table A1.VI. *Raw data of the axial scanning measurement of the assembly #12323 (x = 0 mm, angle = 0 degrees).*

Height	non-corr N_{Cd} (cps)	Error N_{Cd} (cps)	non-corr $N_{no\text{-}Cd}$ (cps)	Error $N_{no\text{-}Cd}$ (cps)	G	Error G	non-corr A_{37} (cps)	Error A_{37} (%)	non-corr $A_{34,605}$ (cps)	Error $A_{34,605}$ (%)	non-corr $A_{34,795}$ (cps)	Error $A_{34,795}$ (%)	non-corr A_{34}/A_{37}
4375	30.42	0.55	50.20	0.71	304.6	0.0775	108.5	1.2	4.5	13.1	3.9	7.8	0.0360
4755	199.13	1.41	313.50	1.77	579.4	0.313	176.2	1	15.5	6.3	9.8	5.8	0.0703
5135	304.27	1.74	484.32	2.20	642.5	0.313	200.9	0.9	17	6.3	13.8	4.3	0.0722
5515	342.05	1.85	544.71	2.33	653.1	0.313	201.4	0.9	19.5	5.4	12.9	4.7	0.0782
5705	352.90	1.88	561.52	2.37	651.9	0.313	190	1	19.4	5.7	13.6	4.4	0.0837
5895	341.00	1.85	546.27	2.34	640.6	0.313	176.5	1	17.1	5.9	12.7	4.8	0.0806
6275	346.82	1.86	561.16	2.37	636.9	0.313	186.6	1	18.8	5.5	13.6	4.5	0.0833
6655	328.25	1.81	526.11	2.29	619.4	0.313	176.5	1	15.9	6.5	12.9	4.5	0.0768
7035	268.19	1.64	426.89	2.07	571.9	0.313	156	1	16	5.9	11.2	4.9	0.0841
7415	148.46	1.22	243.39	1.56	471.3	0.313	131.5	1.1	11.2	7.3	7.7	6.2	0.0695
7795	19.63	0.44	33.26	0.58	254.8	0.0775	82.1	1.3	4.4	12.2	3.1	9.2	0.0440

^{244}Cm NEUTRON SOURCES CALCULATED WITH ORIGEN-S **ANNEX 2**

Table A2.I. *^{244}Cm neutron source (n/s/assembly) dependence on enrichment and burnup at discharge calculated with ORIGEN-S. Void fraction is 0.5.*

Enrichment (w-%)	Burnup (MWd/kgU)					
	15	20	25	30	35	40
1.6	7.21E+06	2.58E+07	6.50E+07	1.31E+08	2.29E+08	3.59E+08
2.0	4.58E+06	1.73E+07	4.60E+07	9.70E+07	1.76E+08	2.86E+08
2.4	3.05E+06	1.20E+07	3.31E+07	7.24E+07	1.36E+08	2.27E+08
2.8	2.12E+06	8.63E+06	2.44E+07	5.47E+07	1.05E+08	1.81E+08
3.2	1.53E+06	6.36E+06	1.84E+07	4.20E+07	8.26E+07	1.45E+08
3.6	1.13E+06	4.80E+06	1.41E+07	3.28E+07	6.56E+07	1.17E+08
4.0	8.61E+05	3.70E+06	1.10E+07	2.60E+07	5.26E+07	9.49E+07
4.4	6.68E+05	2.91E+06	8.77E+06	2.09E+07	4.27E+07	7.78E+07